

Hollow surface nano axial photonic cavities for microfluidic sensing

Samar Deep

A Thesis
in
The Department
of
Physics

Presented in Partial Fulfillment of the Requirements
for the Degree of
Master of Science (Physics) at
Concordia University
Montréal, Québec, Canada

January 2022

© Samar Deep, 2022

CONCORDIA UNIVERSITY
School of Graduate Studies

This is to certify that the thesis prepared

By: **Samar Deep**

Entitled: **Hollow surface nano axial photonic cavities for
microfluidic sensing**

and submitted in partial fulfillment of the requirements for the degree of

Master of Science (Physics)

complies with the regulations of this University and meets the accepted standards
with respect to originality and quality.

Signed by the Final Examining Committee:

_____ Chair
Dr. Valter Zazubovits

_____ Examiner
Dr. Valter Zazubovits

_____ Examiner
Dr. Laszlo Kalman

_____ Supervisor
Dr. Pablo Bianucci

Approved by _____
Dr. Valter Zazubovits, Chair
Department of Physics

_____ 2022

_____ Dr. Pascale Sicotte, Dean
Faculty of Arts and Science

Abstract

Hollow surface nano axial photonic cavities for microfluidic sensing

Samar Deep

Optical cavities are important parts of many scientific and industrial instruments and have been widely studied in the field of optics and photonics. The Surface nanoscale axial photonic (SNAP) cavity, a whispering gallery mode (WGM) type optical cavity has recently gained attention and became the focus of active research. In this thesis we present our work to make a thin-walled hollow SNAP cavity by using a hydrogen torch and a tapered microfiber (TMF) pulling setup. Our method does not require a carbon dioxide laser nor hydrogen fluoride etching. We use a tapered microfiber to excite localized optical resonant modes in the walls of this cavity. We show that when the walls of the capillary are thin enough (10 microns), the electric field from resonance mode extends beyond the internal walls of the cavity and interacts with the medium (air or water) inside the cavity. This shows a proof-of-concept that the thin-walled hollow SNAP cavities can be used as an optical microfluidic sensor. We also measure the transmission impulse response and light pulse dynamics of a SNAP optical cavity using an optical backscatter reflectometer. From the data we compute the lifetime of the light in the SNAP cavity in the time domain, and its round trip time.

Acknowledgments

First and foremost, I would like to extend my deepest gratitude to my research supervisor Dr. Pablo Bianucci. Thank you for your patience, guidance, and support. Whenever I needed help or advice, the door to your office was always open. I have benefited greatly from your wealth of knowledge and meticulous editing. I am extremely grateful that you took me on as a student and continued to have faith in me over the years.

I want to thank the other members of my supervisory committee as well, Dr. Valter Zazubovits and Dr. Laszlo Kalman for their valuable advice and suggestions. Their encouraging words and thoughtful feedback have been very important to me.

I would also like to take this opportunity to thank and acknowledge the support I received from the Lorraine Gosselin Scholarship in Physics, the Hydro-Quebec Master's Scholarship, and Concordia University.

To my past and present fellow research group members, Dr. Xin Jin, Sulman Zia, Alexis Hotte-Kilburn, Rajni Bagga, Dr. Seyed Mohammed Mirjalili, Tabassom Hamidfar, and Mathieu Couillard, thank you for making my time at Concordia interesting and pleasant.

I also want to acknowledge and thank the other faculty members, students, and staff in the department of physics whose help or advice has always been invaluable. Hannes Hase, Israel Gomez Rebollo, Matthew Storms, Dr. Nima Nateghi, Dr. Ingo Salzmann, Marie-Anne Cheong Youne, Zeljko Bulut, Dr. Patrick Doane, and Wentworth Brookes, thank you for helping me on many occasions.

Finally, I could not have completed this thesis without the love and support of my wife Patricia, and my children, Stephen, Sushmita, and Sonia. You gave me motivation and hope. Without you I would not have come this far, thank you.

Contents

List of Figures	vii
List of Tables	xi
List of Abbreviations	xii
1 Introduction	1
1.1 Contributions	2
1.2 Thesis Outline	3
2 Whispering gallery modes (WGM) optical cavity	4
2.1 Whispering gallery modes	5
2.1.1 Properties of a WGM optical cavity	12
2.2 Surface nano axial photonic (SNAP) cavity	12
2.2.1 SNAP cavity	12
2.2.2 Properties of a SNAP cavity	17
2.2.3 Coupling of light into a SNAP cavity	17
2.2.4 Fabrication of the TMF and SNAP cavities	21
3 Proof-of-concept optical sensor using a thin-walled hollow WGM cavity	25
3.1 WGM resonance as a mechanism for Sensing	25
3.2 Thin walled hollow WGM cavity for an optical sensor	27
3.3 Pulling a thin walled hollow WGM cavity from a capillary	29
3.4 Thin walled hollow WGM cavity as an water sensor	36
4 Transmission impulse response and light pulse dynamics of a WGM optical cavity	39
5 Conclusion	46

List of Figures

Figure 2.1	The Whispering Gallery Modes. (a) The Whispering Gallery of St Paul’s Cathedral, London (Image[22]). (b) The Lord Rayleigh (1842 - 1919) (Image[23]). (c) Reflection of sounds waves by gallery walls.	5
Figure 2.2	Resonance modes of optical waves in a dielectric micro ring optical cavity. The plot shows the amplitude of the electric field, where red is positive amplitude, white is zero amplitude, and blue is negative amplitude.	6
Figure 2.3	Total Internal Reflection. Total internal reflection (TIR) of light occurs when $\theta_i > \theta_c$ and the light ray is trapped inside the cavity due to the circular symmetry of the cavity.	7
Figure 2.4	Coupling of light into a WGM micro ring optical cavity by an optical waveguide. The evanescent field from the light traveling through the waveguide excites resonant modes in micro ring. a is the single-pass amplitude transmission. It is related to the loss of light in the cavity during a round trip. r is the self-coupling coefficient, the fraction of the amplitude of the light that continues to the waveguide. k is the cross-coupling coefficient, the fraction of the amplitude of the light that goes into the ring.	8
Figure 2.5	Intensity transmission of a waveguide coupled to a micro ring or a micro disc optical cavity under three different couplings. (a) Under coupled. (b) Critical coupled. (c) Over coupled.	10
Figure 2.6	A micro ring optical cavity coupled to two waveguides and it’s transmission spectrum. The light is coupled into the cavity by one waveguide. The transmission spectrum (blue color) of this waveguide is collected at the photodiode (P). The light that was coupled and stored in the cavity is collected by a second waveguide and sent to the photodiode (D) (red color transmission spectrum).	11

Figure 2.7	A micro ring and a micro disk optical cavities and their extension into microfiber and micro capillary. microfiber (b) 3D optical cavity can be considered a 3D extension of micro disk (a) optical cavity. Similarly, micro capillary (d) 3D optical cavity can be considered a 3D extension of micro ring (c) optical cavity.	13
Figure 2.8	Nano scale surface optical cavities in a optical fiber. (a) and (b) coupling of light by a tapered microfiber (TMF). (c) Slow propagation of light in the axial direction perpendicular to the ring plane (we define this direction as the z-direction). (d) Axial confinement of light by nanoscale barriers called turning points.	14
Figure 2.9	Confinement of light in nano scale surface optical cavities (image reproduced from the article [27]). (a) The confinement of light in the quantum well formed by the nanoscale variation of the effective fiber radius. (b) The confinement of light due to the localization under the potential barrier formed by the neck of the fiber (variation of the fiber radius). (c) The confinement of light near a turning point where the fiber has a monotonically increasing radius. Light is confined between the TMF and the barrier due to destructive interference of light on the other side of the TMF.	16
Figure 2.10	Cavity light coupling and characterization setup. Arrows point to the direction of the flow of the signal. Red is an optical signal, and blue is an electrical signal.	18
Figure 2.11	Cavity positioning and light coupling. Inset: Optical microscope view of the optical cavity and the coupling TMF.	20
Figure 2.12	The image shows the graphical user interface of the precision positioner control software. Control software allows control of the precision positioner in three directions with the step size as small as 1 nm.	21
Figure 2.13	Making a TMF and a SNAP from a single mode telecom optical fiber. (a) Telecom optical fiber, (b) TMF, and (c) SNAP.	22
Figure 2.14	Making a tapered fiber from a telecom optical fiber using a TMF pulling setup.	23
Figure 2.15	Formation of nano scale surface optical cavities on the surface of a pulled telecom fiber. When the pulling stops, the tension in the fiber surface is released and nanoscale variations in the fiber surface are formed.	24

Figure 3.1	WGM resonance sensing mechanism.	26
Figure 3.2	Testing a sample safely inside a micro capillary. Sample under test, gas or liquid, is safely tested inside the capillary while optical components stay outside completely separated from the sample. . . .	28
Figure 3.3	Pulling a thin-walled hollow SNAP cavity on a TMF pulling setup. (a) shows the alignment of the hydrogen torch needle to the capillary from top view. (b) alignment of the hydrogen torch needle to the capillary from front view.	29
Figure 3.4	The thin-walled hollow SNAP cavity pulling recipe.	30
Figure 3.5	Hydrogen oxygen mass flow controller.	31
Figure 3.6	Pulling a Thin-walled hollow SNAP cavity from a off-the-shelf micro capillary. The capillary is pulled on a TMF setup over a hydrogen torch. Flame from the torch softens the capillary. As the capillary is pulled, the material from the walls draws outwards and wall thickness and capillary diameter is reduced. When the pulling stops, tension in capillary walls is released and nanoscale variations in the wall surface are formed.	32
Figure 3.7	Light coupling and testing hollow SNAP cavity. Light was coupled using a TMF. To fill the capillary with the water a drop of water at room temperature was introduced at one end of the capillary and water was sucked in due to the capillary action.	33
Figure 3.8	Pulled micro capillary with reduced diameter and reduced wall thickness. The outside diameter was reduced to approximately 48 micrometers, and the wall thickness was reduced to approximately 10 micrometers.	34
Figure 3.9	Tapered micro fiber pulling recipe.	35
Figure 3.10	Resonance mode shift from water. Spectra of localized modes in a pulled capillary with and without water. Top panel: Spectrum of the empty capillary. Bottom panel: Spectrum after the capillary is filled with water. One of the arrows indicates the mode that is interacting with water.	36
Figure 4.1	Impulse response and light pulse dynamics measurement setup.	40
Figure 4.2	A simplified internal diagram of an optical backscatter reflectometry (OBR) measurement device.	41

Figure 4.3 Transmission impulse response of a SNAP cavity. Top panel shows the transmission amplitude of the light sent out by the OBR that came back to the OBR. When we zoom on the peak as shown in the bottom panel, we see the response of the cavity coupled to the tapered microfiber. 42

Figure 4.4 Transmission impulse response and light pulse dynamics measurement of a SNAP cavity. After every round trip, part of the light that is coupled into the cavity couples out of the cavity by coupling back to the tapered microfiber, this is why we see slowly decaying peaks in the transmission spectrum. Peaks are spaced in time, and the time difference between peaks represents the round trip time of the light traveling inside the cavity. 43

Figure 4.5 Collecting cavity response at nine locations 0.2 millimeters apart. 44

Figure 4.6 Transmission impulse response of a SNAP cavity at nine locations 0.2 mm apart. From bottom to top, transmission from location one at bottom and from nine at the top. At locations eight and nine (top two curves), the fiber does not have any cavity to confine the light; therefore there is no light coupled into these two locations. . 44

List of Tables

Table 2.1	Components of the characterization setup.	19
Table 3.1	The parameters of modes 1, 2, and 3 before and after the capillary is filled with water. Modes 1 and 3 have the blue shift of approximately 8 pm and 7.5 pm. Mode 2, that is interacting with water has a higher blue shift, approximately 10.5 pm. Q reduction is the Q reduction factor.	37

List of Abbreviations

CCW Counterclockwise

CW Clockwise

FSR Free spectral range

FWHM Full width half maximum

IPA Isopropyl alcohol

Q-factor Quality factor

SLPM standard liters per minute

SNAP Surface Nanoscale Axial Photonics

TIR Total internal reflection

TMF Tapered Micro Fiber

WGM Whispering Gallery Modes

Chapter 1

Introduction

The use of optical cavities to confine the light is a very important and widely studied topic in the field of optics and photonics. Optical cavities have become essential parts of many scientific and industrial instruments. Whispering gallery mode (WGM) cavities that use total internal reflection to confine the light have found many uses in both applied and fundamental scientific research, ranging from biomedical sensing to cavity quantum electrodynamics [1–7].

Surface Nanoscale Axial Photonic (SNAP) optical cavities, WGM-type optical cavities have recently gained attention and became the focus of active research[8–14]. These optical cavities support high Q-factor modes, and can produce dispersion-less spectra[15–17] where the frequency of the resonant modes is equally spaced like an ideal optical resonator. Due to these properties, these cavities have shown potential for applications as dispersion-free delay lines, optical buffers, and frequency comb generators [18–20].

1.1 Contributions

In this thesis we contributed to the research on SNAP cavities. We developed an alternate simpler method to fabricate hollow SNAP cavities with a wall thickness less than 10 micrometers, without the use of Carbon dioxide (CO_2) laser or Hydrogen fluoride (HF) etching. Our method uses a simple jeweler's hydrogen-oxygen torch and inexpensive off-the-shelf micro capillaries. Once the hollow SNAP cavity is fabricated, we then use a tapered microfiber to excite localized optical resonant modes in its walls, and use these modes to detect the presence of water inside the capillaries.

This presents the use of a SNAP cavity to make a first-stage proof-of-concept optical sensor. Results from transmission spectroscopy show that our thin walled hollow SNAP cavities can have resonance modes and the walls of the SNAP are thin enough that the resonant modes extend beyond the walls of SNAP and interact with the water.

Next we present the observed light pulse dynamics in SNAP optical cavity. We used an optical circulator to feed back the transmission of a SNAP optical cavity to an Optical Backscatter Reflectometer (OBR) to measure the transmission impulse response (time-domain analysis). The experiment allows us to measure the lifetime of the light in the SNAP cavity, and the result of the measurement shows that part of the light coupled into the SNAP cavity couples out of the cavity by coupling back to the tapered microfiber after every round trip.

1.2 Thesis Outline

This thesis comprises five chapters.

Chapter 1 (the present chapter) provides a general introduction, contributions and the thesis outline.

In chapter 2, we briefly present the literature review and the theoretical background of SNAP devices, including an analogy to quantum mechanics concerning the confinement of light.

In chapter 3, we describe the fabrication of a thin-wall hollow SNAP device using a glass capillary and hydrogen torch brazing, and use it to make a proof of concept optical sensor that detects the presence of water inside the capillary.

In chapter 4, we describe the relationship of the transmission spectrum to the optical impulse response (time-domain analysis) of SNAP optical cavity. We also briefly describe the set-up used to perform these measurements.

In chapter 5, we present the conclusions of this thesis and suggestions for future research.

Chapter 2

Whispering gallery modes (WGM) optical cavity

The term Whispering gallery mode (WGM), as the name suggests, comes from the phenomena known about the gallery of St. Paul's cathedral (figure 2.1(a)) that, if you whisper close to the gallery walls, a person standing across the gallery close to the walls could hear you. The reason behind this phenomenon was first experimentally discovered[21] by Lord Rayleigh (figure 2.1(b)) in 1910. As shown in the figure 2.1(c), Lord Rayleigh explained that sound waves are reflected by the concave walls of the gallery and travel across it.

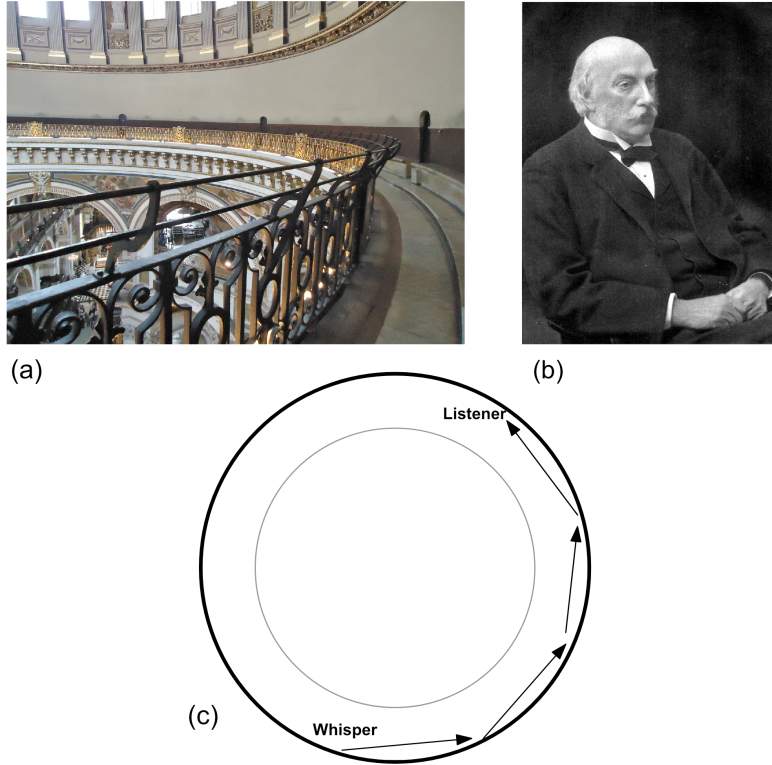


Figure 2.1: The Whispering Gallery Modes. (a) The Whispering Gallery of St Paul's Cathedral, London (Image[22]). (b) The Lord Rayleigh (1842 - 1919) (Image[23]). (c) Reflection of sounds waves by gallery walls.

2.1 Whispering gallery modes

The phenomenon discovered by Lord Rayleigh in the gallery of St. Paul's cathedral is not unique to acoustic waves, but could also be applied to electromagnetic waves in suitably shaped dielectric medium[24]. Figure 2.2 shows the electromagnetic field pattern of resonance modes of optical waves in a dielectric micro-ring optical cavity simulated in COMSOL physics simulation software.

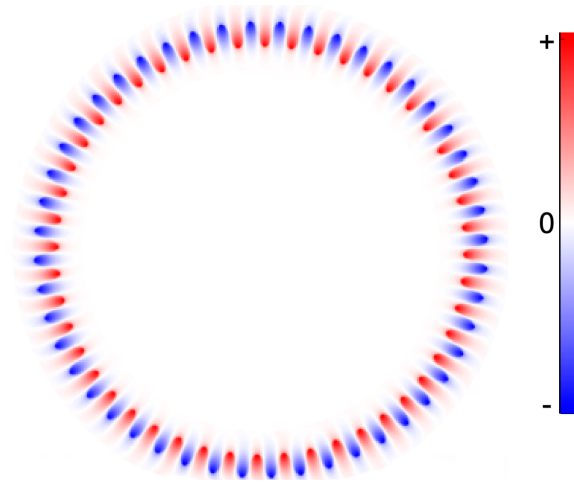


Figure 2.2: Resonance modes of optical waves in a dielectric micro ring optical cavity. The plot shows the amplitude of the electric field, where red is positive amplitude, white is zero amplitude, and blue is negative amplitude.

Consider a circular dielectric cavity such as a micro disc (figure 2.3) or a micro ring, with refractive index of n placed in the vacuum. A light ray of wavelength λ is coupled into the cavity. The light ray propagates inside the cavity hitting the cavity surface with an angle of incidence θ_i . The dielectric circle has a radius r with $r \gg \lambda$.

Total internal reflection (TIR) of light occurs when $\theta_i > \theta_c$ and the light ray is trapped inside the cavity due to the circular symmetry of the cavity. Here θ_c is the critical angle, defined as $\theta_c = \arcsin(1/n)$. If the light ray travels close to the cavity surface at near-glancing angle ($\theta_i \approx \pi/2$), in a round trip it covers an approximate distance of $2\pi r$ or an optical path length of $2\pi r n$ in a round trip.

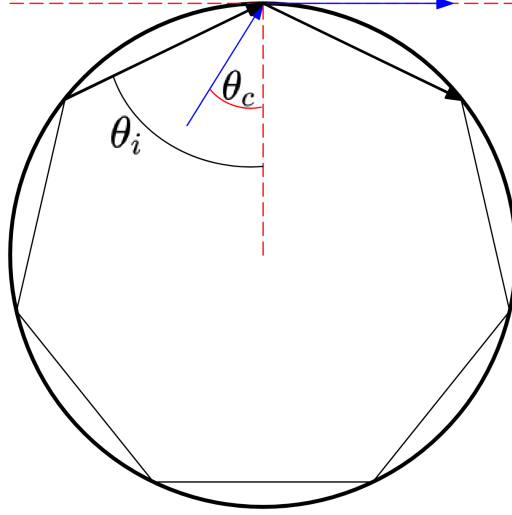


Figure 2.3: Total Internal Reflection. Total internal reflection (TIR) of light occurs when $\theta_i > \theta_c$ and the light ray is trapped inside the cavity due to the circular symmetry of the cavity.

When this optical path length exactly equals an integer ℓ number of wavelengths in the cavity, phase matching occurs after a round trip and the light ray interferes with itself constructively, leading to the resonance modes in the cavity. Equation (eq. 1) gives the condition when satisfied along with TIR leads to resonance.

$$\text{Resonance Condition :} \quad 2\pi r n_c = \ell \lambda \quad (1)$$

Since the momentum p of a photon is $p = \hbar k$, and $k = 2\pi n_c / \lambda$ is the wavenumber, the number of wavelengths ℓ can also be identified as the angular momentum of light circulating close to the surface inside the cavity ($\hbar \ell = r p = r \hbar 2\pi n_c / \lambda$). These resonances in the optical cavity are a function of cavity morphology and dielectric properties of the cavity and its surroundings. Any change in any of these parameters will lead to a change in the resonance, and as shown in the next chapter, this can be exploited to use a WGM optical cavity as a sensor.

The above example uses one wavelength to show the existence of resonant modes, but in fact WGM cavities support multiple resonances. There are multiple wavelengths that can fit an integer number of time and be resonant. The spacing between these resonances is called the free spectral range (FSR)[25] of the cavity.

$$FSR = \frac{\lambda^2}{2\pi r n_c} \quad (2)$$

FSR is also the inverse of a time that light takes to make a round trip. Considering that light travels distance $2\pi r$ inside the cavity at the speed of c/n , it will take a time $T_r = 2\pi r n/c$ to make a round trip.

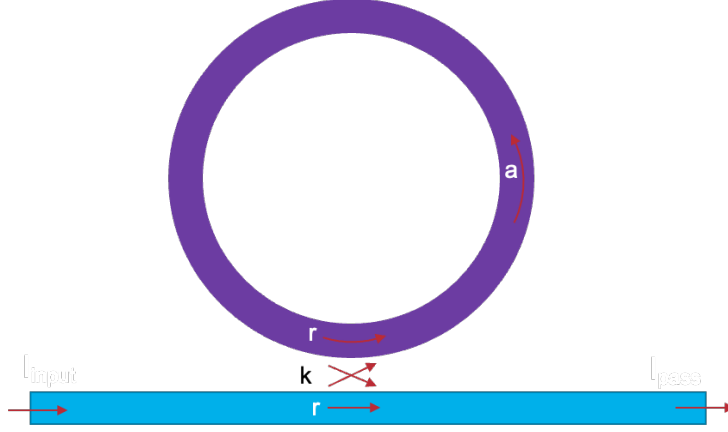


Figure 2.4: Coupling of light into a WGM micro ring optical cavity by an optical waveguide. The evanescent field from the light traveling through the waveguide excites resonant modes in micro ring. a is the single-pass amplitude transmission. It is related to the loss of light in the cavity during a round trip. r is the self-coupling coefficient, the fraction of the amplitude of the light that continues to the waveguide. k is the cross-coupling coefficient, the fraction of the amplitude of the light that goes into the ring.

Figure 2.4 shows the coupling of light into a micro ring optical cavity. Light is coupled into the micro ring by an optical waveguide. An optical waveguide uses TIR to guide laser light through it. As the light travels through the waveguide, evanescent field from the light surrounds the waveguide and excites the modes in micro ring. The output of the waveguide is collected by a photo detector. Wavelengths that match the resonance conditions are coupled in the cavity and a dip in waveguide transmission is produced.

Equation 3 [26] defines the intensity transmission of a waveguide coupled to a micro ring or a micro disc cavity.

$$T = \frac{I_{\text{pass}}}{I_{\text{input}}} = \frac{a^2 - 2ra \cos \phi + r^2}{1 - 2ar \cos \phi + (ra)^2} \quad (3)$$

In this equation, ϕ is the single-pass phase shift and defined as the product of round trip length $2\pi r$ and the propagation constant of the circulating mode inside the cavity.

The propagation constant of the circulating mode is related to the spatial variation of the electromagnetic field along the direction of propagation. More specifically, it describes the spatial evolution of the phase as the light propagates along the waveguide. Resonance in the cavity occurs when the phase ϕ is a multiple of 2π , or, in other words, when the wavelength of the light fits an integer number of times inside the cavity.

The single-pass amplitude transmission a is related to the loss of light in the cavity during a round trip. It is defined as $a = \sqrt{\exp(-\alpha x)}$. Where x is the round trip length ($x = 2\pi r$) and α is the power attenuation coefficient defined in units of $[1/cm]$. Power attenuation or loss of energy in the waveguide arises from both radiative and not radiative process, for example scattering from the rough cavity surface or absorption by the cavity medium.

In equation 3, r is the self-coupling coefficient, and k is the cross-coupling coefficient. The self-coupling r is the fraction of the amplitude of the light that continues to the waveguide, and the cross-coupling k is the fraction of the amplitude of the light that goes into the ring. Assuming that there are no losses in coupling, r and k are related by the equation $r^2 + k^2 = 1$.

The intensity transmission of equation 3 under three different couplings is plotted in figure 2.5.

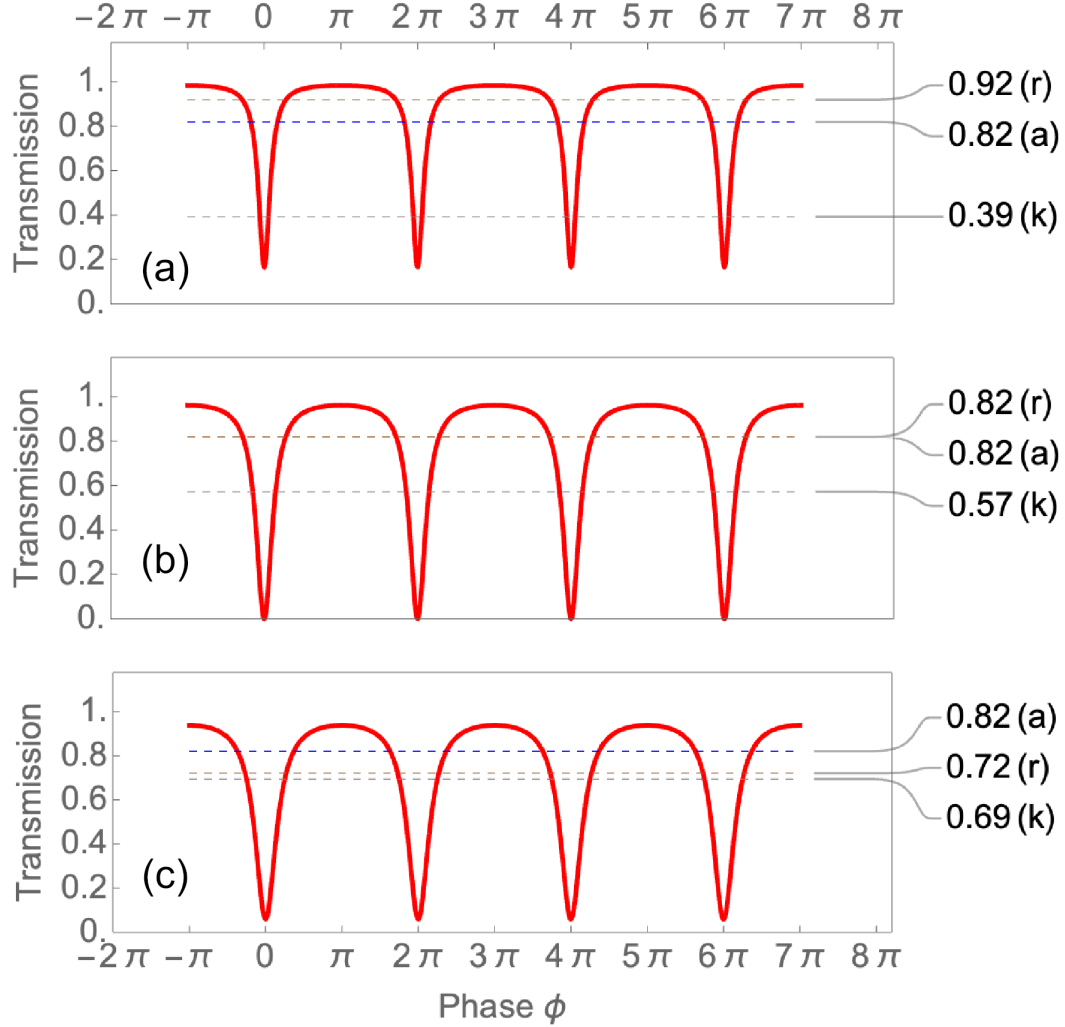


Figure 2.5: Intensity transmission of a waveguide coupled to a micro ring or a micro disc optical cavity under three different couplings. (a) Under coupled. (b) Critical coupled. (c) Over coupled.

When the self-coupling coefficient $r > a$ (figure 2.5(a)), coupling of a waveguide to a cavity is defined as under coupled. When the self-coupling coefficient $r = a$, coupling is defined as critical coupling (figure 2.5(b)). Assuming there are no losses in coupling, critical coupling means that no light of wavelengths that resonate with the cavity (phase ϕ equal to integer number of 2π) pass through the waveguide to the photo detector. Light of these resonance wavelengths is stored and lost inside the cavity and produces the deepest dip in transmission spectrum. When the self-coupling coefficient $r < a$ (figure 2.5(c)), the coupling is called over coupled.

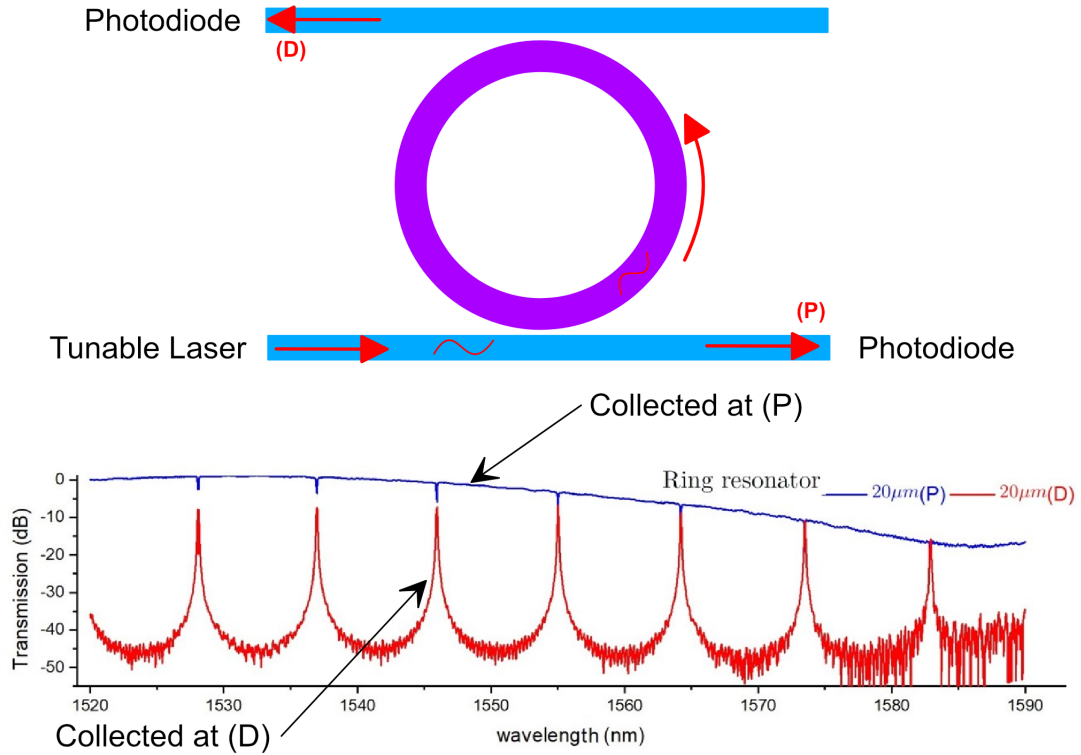


Figure 2.6: A micro ring optical cavity coupled to two waveguides and its transmission spectrum. The light is coupled into the cavity by one waveguide. The transmission spectrum (blue color) of this waveguide is collected at the photodiode (P). The light that was coupled and stored in the cavity is collected by a second waveguide and sent to the photodiode (D) (red color transmission spectrum).

Figure 2.6 shows a transmission spectrum of a micro ring optical cavity coupled to two waveguides. In this setup light is coupled into the cavity by one waveguide. The transmission spectrum (blue color) of this waveguide is collected at the photodiode (P). The light that was coupled and stored in the cavity is collected by a second waveguide. The transmission spectrum (red color) of the second waveguide is collected at the photodiode (D). The purpose of this figure is to only show that it's also possible to couple two waveguides to a cavity and retrieve the coupled light, but for the rest of this thesis we will be using only a one cavity and one waveguide setup.

2.1.1 Properties of a WGM optical cavity

The quantities Q-factor and Finesse[25] tell us about the quality of an optical cavity. The Q-factor is a dimensionless parameter and indicates energy loss. As mentioned previously, loss of energy in the waveguide occurs in the form of both radiative and nonradiative processes. The Q-factor is determined by the cavity losses, and it tells us how the line width of a resonance compares to the central wavelength of the resonance.

$$Q = \frac{\lambda}{\Delta\lambda} = \omega_0\tau_c \quad (4)$$

Alternatively The Q-factor is also defined as the product of central frequency of the resonance and the cavity lifetime τ_c of the resonance.

The finesse is defined as the FSR divided by the line width of the resonance at full-width half maximum (FWHM).

$$F = \frac{FSR}{\Delta\lambda} \quad (5)$$

The finesse tells us how the line width of resonance of a cavity compares to the space between resonances. It can be considered as the resolving power. The higher the finesse, the better resolved is the resonance.

2.2 Surface nano axial photonic (SNAP) cavity

Surface nano axial photonics (SNAP) cavity is a WGM cavity created on the surface of a microfiber or a micro capillary by inducing nanoscale deformations in the surface.

2.2.1 SNAP cavity

In a way, a SNAP cavity can be considered a 3D extension of a micro disk (figure 2.7) or a micro ring and coupling of light by optical waveguide is replaced by coupling of light by a tapered microfiber (TMP)(figure 2.8 (a) and (b)). The thickness of a micro disk or a micro ring is typically 50 nm to 220 nm. In these structures light is confined only to the ring plane, and there is no propagation in z direction (we define the z direction as that perpendicular to the ring plane).

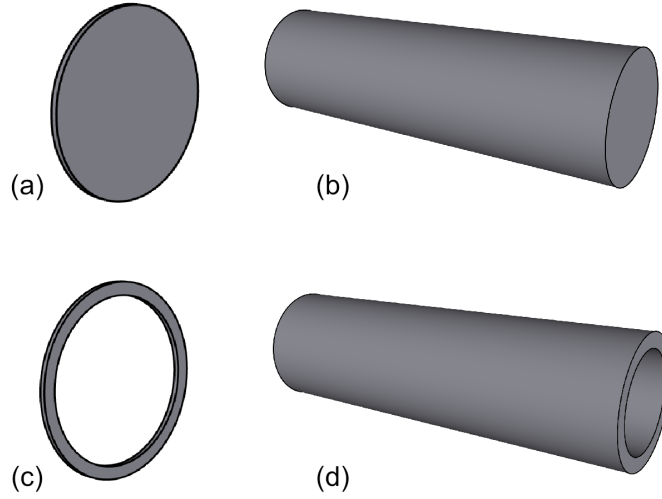


Figure 2.7: A micro ring and a micro disk optical cavities and their extension into microfiber and micro capillary. microfiber (b) 3D optical cavity can be considered a 3D extension of micro disk (a) optical cavity. Similarly, micro capillary (d) 3D optical cavity can be considered a 3D extension of micro ring (c) optical cavity.

If we take one of these structures and extend the thickness into z direction, and if the coupling light has non-zero spatial frequency component in z direction it will propagate slowly in the z direction with the propagation constant close to zero (figure 2.8(c)) until it comes across a barrier and turns back. Barrier is created by nanoscale deformations in the surface (figure 2.8(d)). Light is confined radially due to the circular symmetry of the SNAP cavity and the TIR as in case of micro disk or ring and axially due to these nanoscale barriers called turning points. Even in the absence of barriers it's possible to get axial confinement with no propagation along the z direction but confinement is worst and less robust.

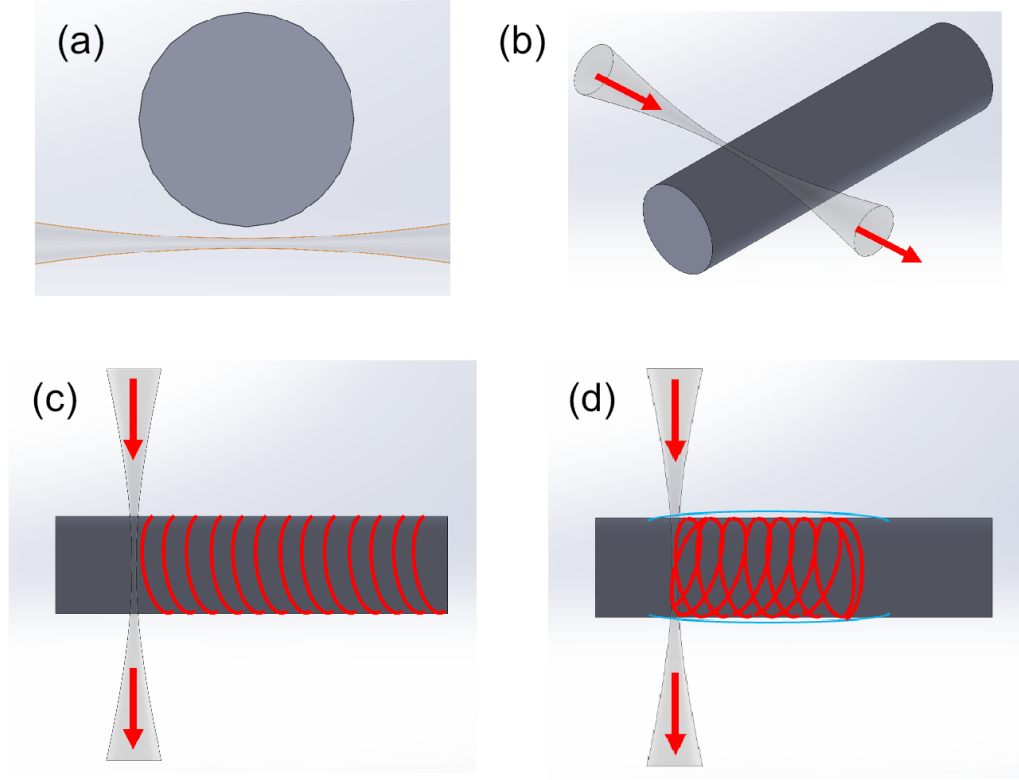


Figure 2.8: Nano scale surface optical cavities in an optical fiber. (a) and (b) coupling of light by a tapered microfiber (TMP). (c) Slow propagation of light in the axial direction perpendicular to the ring plane (we define this direction as the z -direction). (d) Axial confinement of light by nanoscale barriers called turning points.

As illustrated in figure 2.9 confinement of light in a SNAP cavity can be described in three ways[27]. Confinement of light in region one in figure 2.9(a) is similar to a micro bottle cavity. Light is coupled on location z_1 between two nanoscale barriers, z_{t1} and z_{t2} . Light is trapped in this region between the two turning points formed by the nanoscale variation in the effective fiber radius. The situation is analogous to a quantum well, and can be described by the one-dimensional Schrödinger equation [27] with optical parameters,

$$\frac{d^2\Psi(z)}{dz^2} + [E(\lambda) - V(z)]\Psi(z) = 0. \quad (6)$$

The potential well $V(z)$ is proportional to the effective radius variation $\Delta r_{eff}(z)$ along the z -axis, and defined by the variation of the radius and the refractive index,

$$V(z) = -k^2 \Delta r_{eff}(z) \quad (7)$$

where

$$\Delta r_{eff}(z) = \left(\frac{\Delta r(z)}{r_0} + \frac{\Delta n(z)}{n_0} \right) \quad (8)$$

and

$$k = \frac{2\pi n_0}{\lambda_{res}}. \quad (9)$$

The energy E is proportional to the wavelength variation $\Delta\lambda$ and defined as

$$E(\lambda) = -k^2 \left(\frac{\lambda - \lambda_{res}}{\lambda_{res}} \right). \quad (10)$$

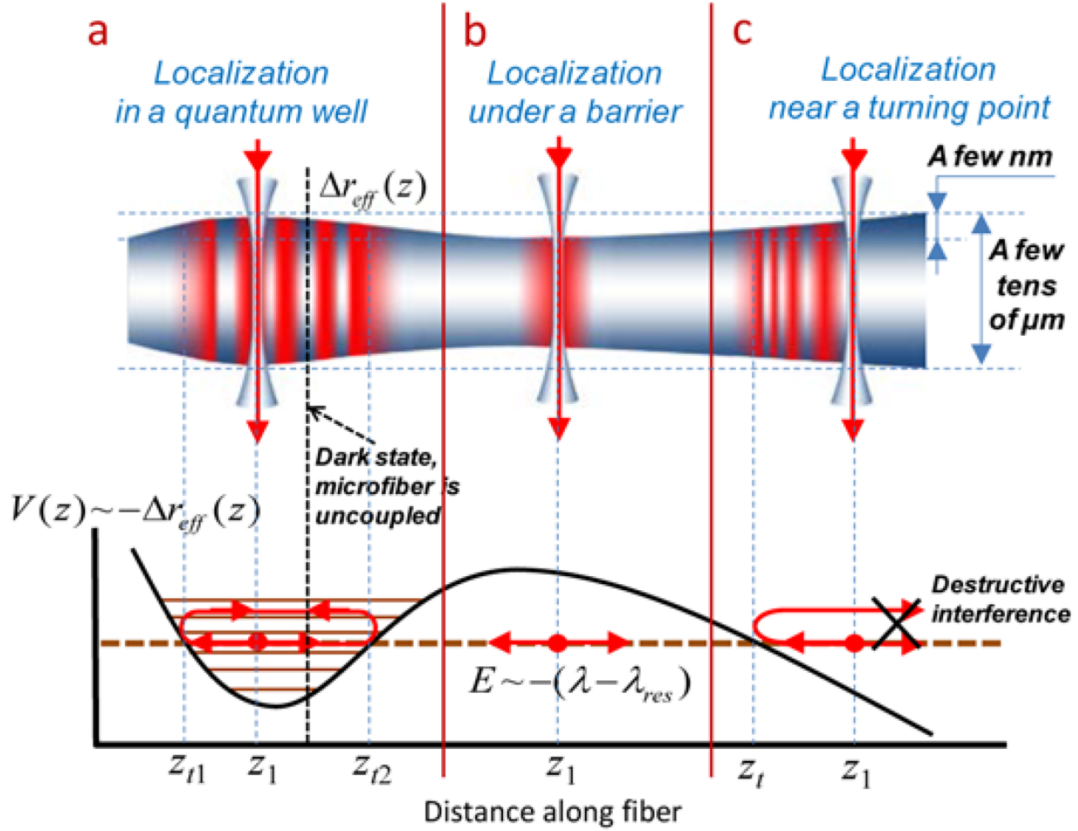


Figure 2.9: Confinement of light in nano scale surface optical cavities (image reproduced from the article [27]). (a) The confinement of light in the quantum well formed by the nanoscale variation of the effective fiber radius. (b) The confinement of light due to the localization under the potential barrier formed by the neck of the fiber (variation of the fiber radius). (c) The confinement of light near a turning point where the fiber has a monotonically increasing radius. Light is confined between the TMF and the barrier due to destructive interference of light on the other side of the TMF.

The evanescent field from the TMF when in contact with the cavity excites WGM modes in the cavity. Light in excited WGM modes moves slowly back and forth between the two turning points, interferes with itself and creates states localized between them. If we place the tapered fiber at the location where it coincides with a node (dark state) in WGM then the coupling to the cavity would not occur and WGM will become dark.

In the second region (figure 2.9(b)) light is confined due to localization under a barrier. The TMF is coupled over a concave barrier (neck of the fiber) and excites

WGM right under the barrier. Light is only confined when there is no wavelength variation. If the wavelength is longer than resonance wavelength, energy will be lower and correspond to the energy found under the barrier. WGM excited in the cavity in this case will decay away from the coupling point. If the wavelength is shorter than resonance wavelength, energy will be higher and correspond to the energy found above the barrier. WGM excited in the cavity in this case will not be localized.

In the third region (figure 2.9(c)) a tapered microfiber excites WGM near a turning point where the fiber has a monotonically increasing radius and light is confined between the TMF and the barrier due to destructive interference of light on the other side of the TMF. The WGM propagating toward the barrier turns back from the barrier and interfere with the modes excited the other side of the fiber and halt the propagation of light in that direction. This destructive interference phenomenon is the same as observed in the combination of light coming out from two arms of a Mach-Zehnder interferometer.

2.2.2 Properties of a SNAP cavity

The quantities (Q-factor and finesse) that define the quality of a micro ring cavity remain the same for a SNAP cavity, and are defined by same equations (4 and 5). In comparison to a micro-ring cavity, a SNAP has longer round trip time and optical path length. Light in a SNAP takes a helical path, slowly propagating in the z direction. Its path is made of multiple circular turns compared to just one in a micro ring. Despite the longer round trip time and longer optical path length per round trip, a SNAP cavity can have longer cavity lifetime and higher Q-factor (up to 10^{11} [28]) than a typical micro ring. SNAP cavities have much smoother surfaces compared to micro rings and very low scattering losses, leading to longer cavity lifetime and high Q-factor. Another advantage of SNAP cavities in comparison to a micro ring is that SNAP cavities are easier, faster, and cheaper to make.

2.2.3 Coupling of light into a SNAP cavity

Coupling of light into a SNAP cavity is done by a TMF [29, 30]. TMF is made from an off-the-shelf standard single mode telecom fiber [31–33]. An off-the-shelf single mode telecom optical fiber has a cladding diameter of 125 microns. In order to introduce a tapered region in the fiber, it is softened by a hydrogen torch and pulled by linear motors so that the waist of the fiber (figure 2.14) is adiabatically reduced to one to three micrometers. Light passing through this tapered region of the fiber

extends through the surface as the evanescent field. When a SNAP cavity is brought in contact with this evanescent field, it excites resonance modes in the cavity [29, 30]. Figure 2.10 illustrates a diagram of a SNAP cavity light coupling and characterization setup.

A C+L band tunable lasers provides linearly polarized laser light ranging from 1500 nm to 1600 nm. The laser optical output is sent to an isolator, whose function is to protect the laser from any reflections that might come back from optical circuit. It essentially allows the light to travel in only one direction. The laser also sends an electronic signal to an oscilloscope indicating when a wavelength sweep starts and ends as the laser cycles through it.

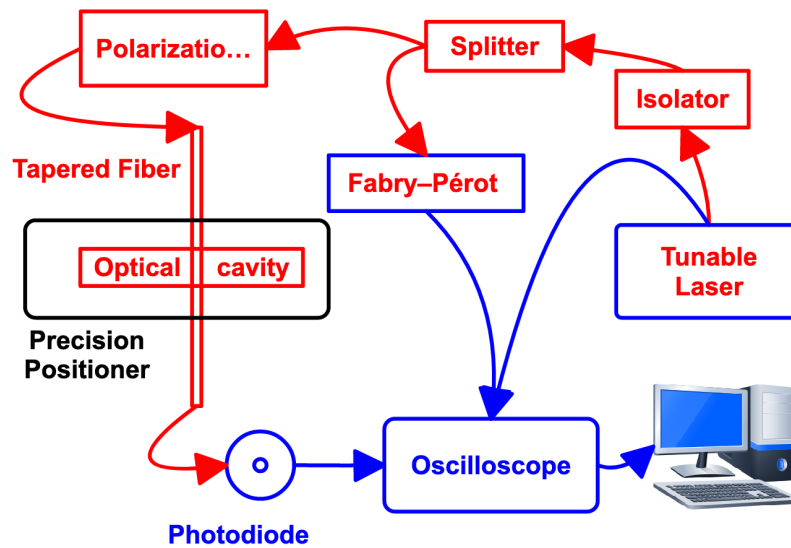


Figure 2.10: Cavity light coupling and characterization setup. Arrows point to the direction of the flow of the signal. Red is an optical signal, and blue is an electrical signal.

	Component	Make	Model
1	Tunable Laser	GN-Nettest	TUNICS-plus 3644HE-15
2	Oscilloscope	Tektronix	MDO 4034
3	Fabry-Perot Wavelocker	JDS Uniphase	FPWL 211501100
4	Splitter	Fiber Optics Communications Inc.	C-WS-AL-05-S-1210-15-AP/AP
5	Isolator	E-TEK	IWDMA410CRV 06
6	Fiber Polarization Controller	OZ Optics	FPC - 100
7	Photo-diode Detector	Thorlabs	PDA - 10CF
8	Optical Microscope	Veho	VMS - 460
9	Precision Positioner	Micronix USA	PPS - 20 (x3)

Table 2.1: Components of the characterization setup.

From the isolator, light is sent to a splitter which splits the light into the ratio of 95% and 5%. The output from the 95% port is sent to a polarization controller. The purpose of the polarization controller is to mitigate any changes to the polarization that might have occurred due to stress and strain in the optical fiber, and to selectively rotate the linearly polarized light so that when the light is coupled into the SNAP cavity, light can be manipulated to be either S or P polarized. The output from polarization controller is sent to the TMF. After that, that laser light from TMF is sent to a photodiode. The photodiode converts the optical signal into electrical one, and this electrical signal is sent to an oscilloscope. The output from the 5% port of the splitter is sent to a Fabry Perot Etalon. This etalon takes the laser light and changes it to an electrical signal and which provides an optical frequency reference at every 100 GHz in the form of an electrical signal in the oscilloscope. The oscilloscope uses the signal from the laser to lock onto the signal from the TMF. Oscilloscope also digitizes all the electric signals it receives and sends them to a computer for data capture and analysis.

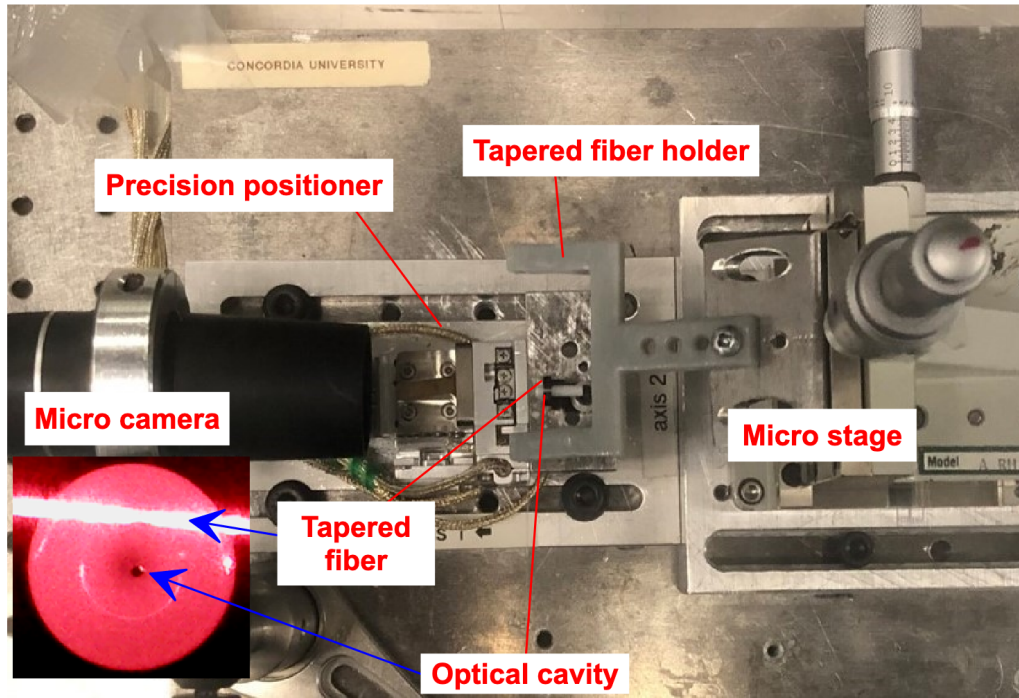


Figure 2.11: Cavity positioning and light coupling. Inset: Optical microscope view of the optical cavity and the coupling TMF.

Figure 2.11 shows the coupling of light into a SNAP cavity. In order to couple light into the SNAP cavity, the TMF is brought into contact with the cavity. Since the TMF at its thinnest part is only few micrometers wide, it is very fragile. Any coarse movement from micro stage after the cavity is touching the TMF will break it. Therefore, TMF is mounted on a computer-controlled precision positioner to make the final contact to the cavity. The SNAP cavity is mounted on a manual micro positioning stage. First the TMF and the cavity are brought closer, within a few millimeters, by moving the manual stage. Then, the computer-controlled precision positioner is used to bring them together. Figure 2.12 shows the graphical user interface of precision positioner control software. Depending on the type of cavity, the mounting of the cavity and the TMF can be switched. The cavity can be mounted on the precision positioner, and the TMF can be mounted on the manual stage. But the process of bringing them together remains the same.



Figure 2.12: The image shows the graphical user interface of the precision positioner control software. Control software allows control of the precision positioner in three directions with the step size as small as 1 nm.

2.2.4 Fabrication of the TMF and SNAP cavities

An off-the-shelf mono single telecom optical fiber is used to make a TMF and a SNAP[31–33]. A single mode telecom optical fiber has a light guiding core, cladding, and a coat to protect the fiber (figure 2.13(a)). The cladding diameter is usually around 125 micrometers, and the core one is 10 microns.

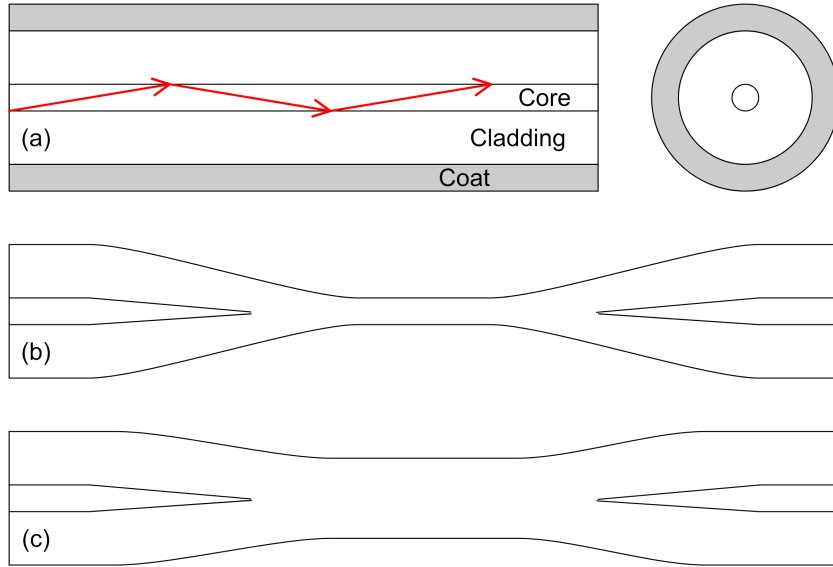


Figure 2.13: Making a TMF and a SNAP from a single mode telecom optical fiber. (a) Telecom optical fiber, (b) TMF, and (c) SNAP.

In order to make a tapered fiber, the coating from the fiber is stripped off and the fiber cladding is cleaned with isopropyl alcohol. The cleaned fiber is mounted on a setup (figure 2.14) made of fiber clamps and linear motors. To introduce a tapered region in the fiber, the flame from a hydrogen torch is used to soften the fiber while linear motors sweep and pull the fiber. The fiber is pulled until the cladding diameter is between one and three microns. As the fiber is pulled, the core disappears, and the tapered region is made of cladding only. The speeds of sweeping and pulling are controlled by a computer program (figure 3.9) and the amount of hydrogen burning is adjusted by a mass flow controller (figure 3.5). Different sets of these parameters, called pulling recipes, can be used to produce different shapes of the fiber's tapered region [31].

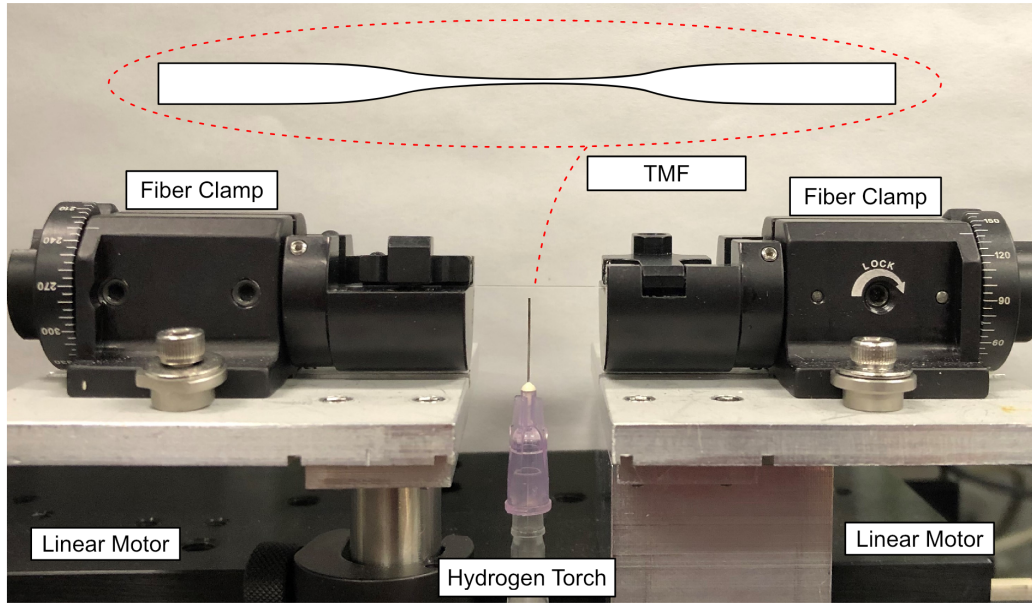


Figure 2.14: Making a tapered fiber from a telecom optical fiber using a TMF pulling setup.

The same TMF making setup is used to make a SNAP cavity with a SNAP pulling recipe[33]. The fiber is softened by sweeping it over a hydrogen torch, and pulled by linear motors until its waist is indicated to be between twenty and thirty microns (figure 2.15). When the pulling stops, tension in fiber surface is released and nanoscale variations in the fiber surface are formed. Figure 2.15 shows the nanoscale variations in the fiber, but these are enlarged for visibility in the image. These variations are so small that they cannot be imaged by a microscope.

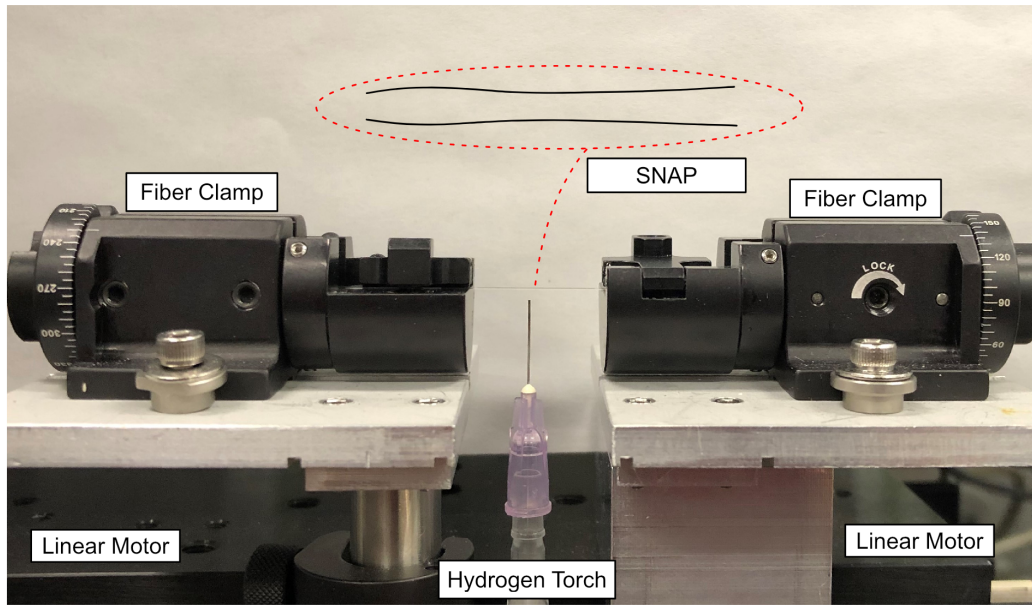


Figure 2.15: Formation of nano scale surface optical cavities on the surface of a pulled telecom fiber. When the pulling stops, the tension in the fiber surface is released and nanoscale variations in the fiber surface are formed.

Chapter 3

Proof-of-concept optical sensor using a thin-walled hollow WGM cavity

The goal of this project was to demonstrate a proof-of-concept optical sensor using a thin-walled hollow WGM cavity. The hollow WGM cavity had to be made of a capillary. The walls of the capillaries were to be thin enough that the evanescent field of resonance modes in the capillary walls would extend inside the capillary and interact with the inner environment. In order to achieve this, walls of the capillary needed to be thinned without using hydrogen fluoride etching and the SNAP cavities were to be induced in capillary walls without using a carbon dioxide laser.

Here we present our work done to pull an off-the-shelf capillary using a TMF puller. We reduced capillary wall thickness by pulling and at the same time induced nanoscale surface optical cavities in capillary walls. Our method does not require a carbon dioxide laser nor hydrogen fluoride etching. Next we used a tapered microfiber to excite localized optical resonant modes in walls, and used these modes to detect the presence of water inside the capillary.

3.1 WGM resonance as a mechanism for Sensing

As mentioned in the previous chapter, resonance modes in a dielectric cavity are a function of the cavity morphology and properties, as well as its surroundings. Due to the fact that SNAP cavities have narrow line width and high Q-factor, even a very small change in the cavity surroundings can lead to a change in resonance modes[34].

Figure 3.1 shows the three fundamental ways in which the resonance modes in a cavity can change in response to changes in the cavity or its surroundings. Depending on what is the target for the detection, an optical sensor based on a WGM cavity could use one or a combination of these three sensing mechanisms.

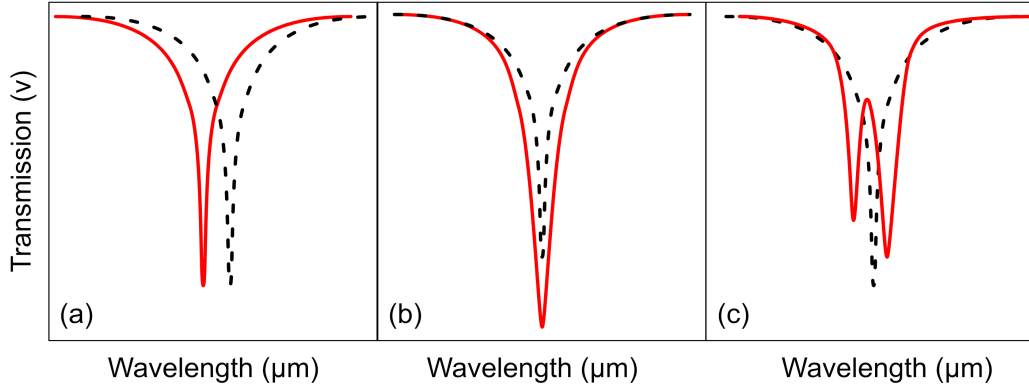


Figure 3.1: WGM resonance sensing mechanism.

- (a) Resonance mode wavelength shift due to the refractive index change,
- (b) resonance line width broadening due to absorption, and
- (c) resonance mode splitting due to a scatterer induced coupling between the clockwise and counterclockwise propagating modes.

Resonance mode wavelength shift (figure 3.1(a)) is the most used WGM sensing mechanism. It has been used to detect the adsorption of single nanoparticles, single molecules, and thin layers of material on the cavity surface [34–36]. For example, a resonance shift occurs if a particle with refractive index higher than the environment around the cavity is adsorbed on the cavity surface. The particle on the surface pulls a part of the optical field towards it, therefore increasing the optical path length of light in the cavity and leading to a resonance mode shift to a longer wavelength (red shift).

Resonance wavelength shifts can also be used to detect the bulk refractive index changes surrounding the cavity or to detect changes in physical parameters such as heat and pressure[37]. For example, an increase in temperature induces thermal expansion and increases the refractive index of the cavity[38] leading to a shift of resonance wavelengths to longer wavelengths. Resonance modes can also shift to a shorter wavelength (blue shift), for example when the refractive index of the medium surrounding the cavity is increased but stays less than the refractive index of the cavity. In this case, the refractive index contrast between the cavity and its surrounding medium is reduced, leading to a reduction in the effective refractive index

of the cavity. This means that the optical path length is reduced and the resonance mode shifts to shorter wavelengths.

Resonance line width broadening (figure 3.1(b)) is another WGM sensing mechanism. Resonance line width broadening occurs due to either absorption or scattering of energy stored in the cavity by nanoparticles, molecules, or changes in the medium surrounding the cavity [39–42]. If the cavity losses increase, the lifetime of energy stored in the cavity will be reduced leading to lower Q-factor and wider resonance line width.

The third WGM sensing mechanism is the resonance mode splitting (figure 3.1(c)). It is mainly used for detecting nanoparticles on the scale of 10-100 nm. In a WGM cavity, resonant modes exist in pairs of clockwise (CW) and counterclockwise (CCW) propagating degenerate modes [43–47]. When scatterers are absorbed on the surface of the cavity, part of the light from the CW mode is scattered by scatterers into the CCW mode and vice versa. This induces the coupling between the two counter-propagating modes and the degeneracy between the two modes is lifted leading to the splitting.

3.2 Thin walled hollow WGM cavity for an optical sensor

Using a hollow thin wall capillary as an optical sensor may have benefits specifically in sensing related to microfluidics. As illustrated in figure 3.2 WGMs in the walls of the capillary interacts with the sample inside, and the sample under test, gas or liquid, can stay contained in the capillary separate from optical components and can be safely tested without the risk of being exposed to the environment or, in case if it's toxic, exposing the environment to it.

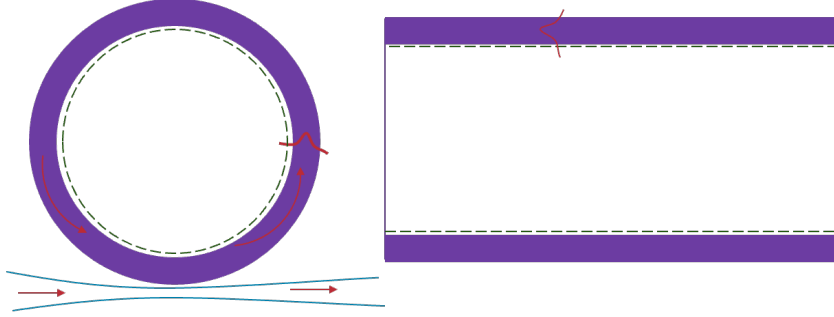


Figure 3.2: Testing a sample safely inside a micro capillary. Sample under test, gas or liquid, is safely tested inside the capillary while optical components stay outside completely separated from the sample.

Since the light ray inside a circular dielectric cavity travels close to the outer cavity surface at near-glancing angle ($\theta_i \approx \pi/2$), most of the energy and resonant modes in a hollow circular dielectric cavity will be concentrated close to the outer surface. If a capillary has the thick wall, resonant modes will not extend beyond the internal surface of the capillary wall and will not interact with the medium inside the capillary[48, 49]. Therefore, for the electric field from the resonance modes to interact with the medium inside the capillary, the capillary wall needs to be thin enough so that the field will not only be confined in the wall of the capillary but also extend beyond the internal surface of the capillary and interact with the medium inside. If the electric field from the resonance modes extends beyond the internal wall, and there is any change in the medium, the resonance mode will react to the change and this can be observed in the cavity transmission signal.

Furthermore, we can functionalize the capillary walls to a specific antibody or agent that will only bind to another very specific target agent. If the target agent is present in solution, it will bind to the antibody leading to a change in the resonance modes in the cavity. For example, this has been used for detection of a very specific bacteria[50] with a micro disk. If we use a thin-walled hollow capillary for a similar experiment then the optical components will not be contaminated by the sample under test.

3.3 Pulling a thin walled hollow WGM cavity from a capillary

In order to make a thin wall hollow SNAP cavity, we used an off-the-shelf micro capillary (Vitrocom borosilicate CV0508). We first cleaned the outer surface of the capillary thoroughly with isopropyl alcohol (IPA). This is very important because if any contamination on the surface remains, it will be burned by the hydrogen flame when pulling the capillary and it will introduce optical losses in the WGMs.

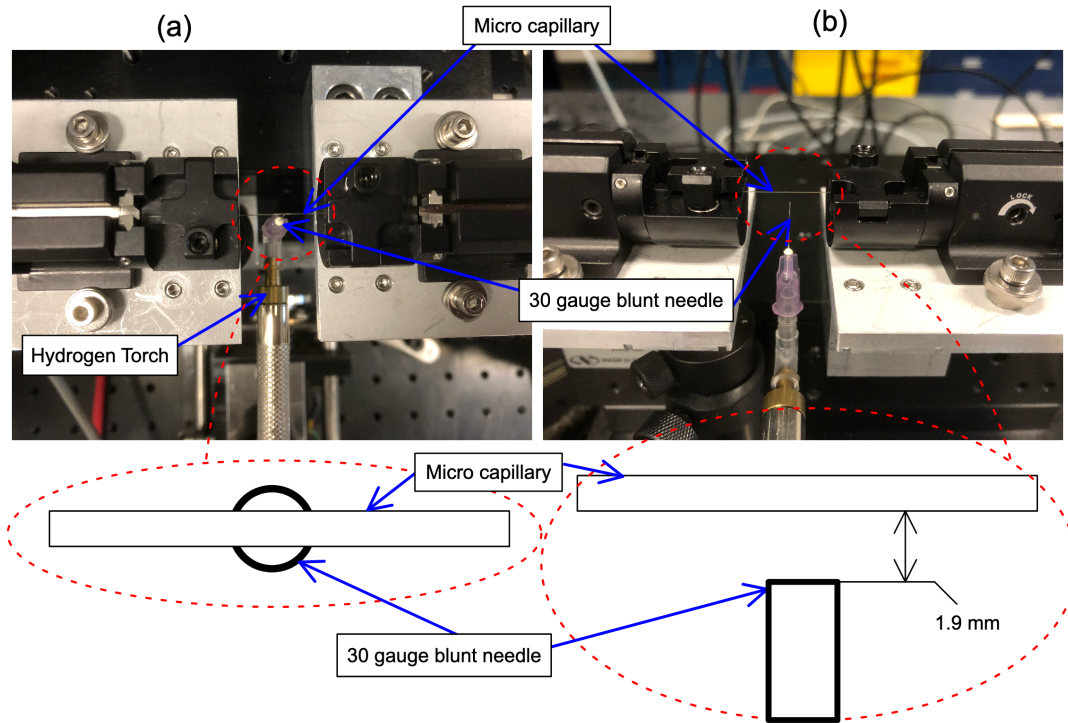


Figure 3.3: Pulling a thin-walled hollow SNAP cavity on a TMF pulling setup. (a) shows the alignment of the hydrogen torch needle to the capillary from top view. (b) alignment of the hydrogen torch needle to the capillary from front view.

We then mounted the capillary on the TMF puller setup that we have in our lab (figure 3.3) and used the pulling recipe given in figure 3.4. The capillary was pulled for 60 seconds at a pulling speed of 0.1 millimeters per second while sweeping the capillary over the flame coming from the hydrogen torch. The capillary was swept at a speed of two millimeters per second with an initial hot zone length of nine

millimeters. The hydrogen torch used a gauge 30 blunt needle to control the size of the flame. The capillary was placed 1.9 millimeters above the needle and aligned to its needle. The flow of hydrogen and oxygen to the torch was 0.012 standard liters per minute (SLPM). Flow was controlled by a mass flow controller (figure 3.5) .

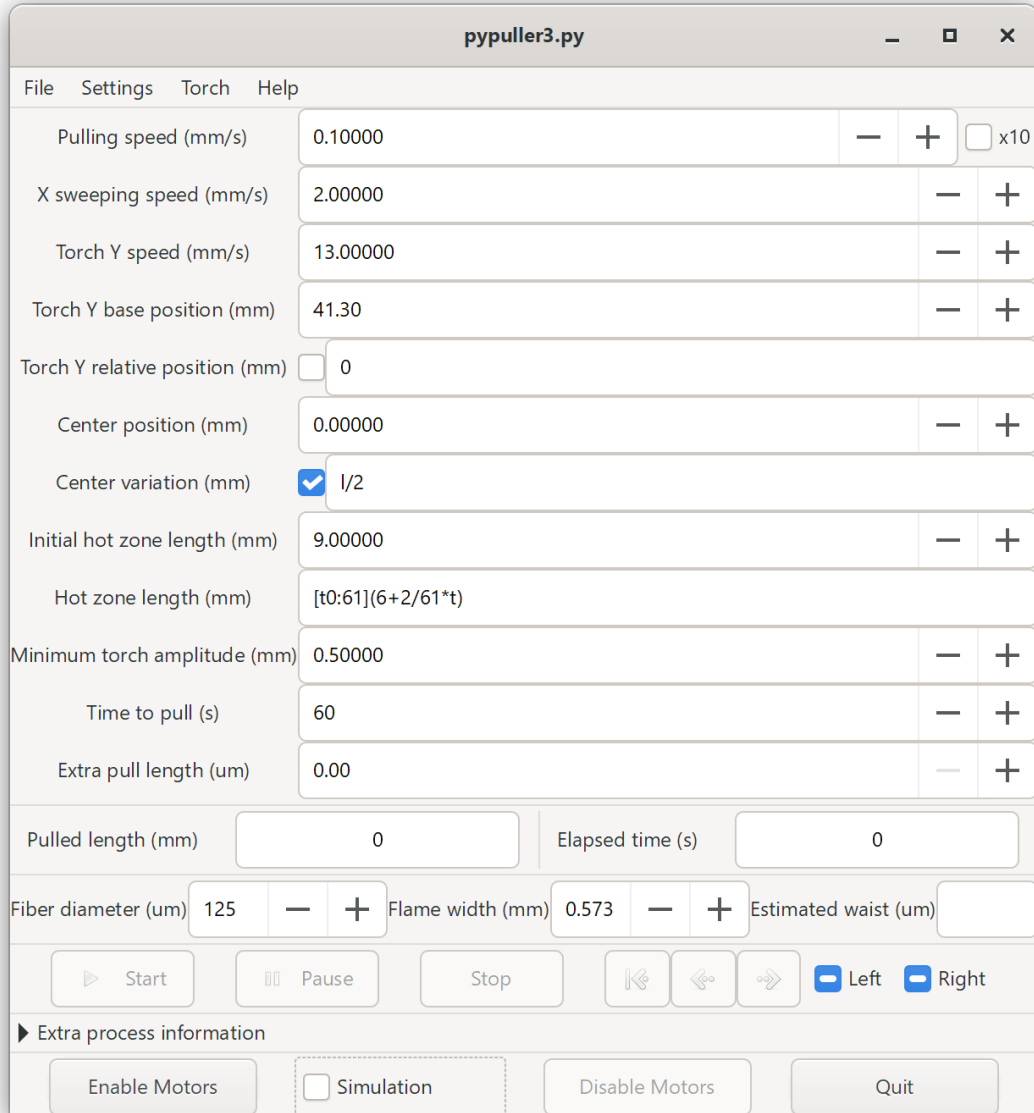


Figure 3.4: The thin-walled hollow SNAP cavity pulling recipe.

It is important to note that the mass flow rate used to pull the capillary is only a quarter of what is usually used to pull a TMF. When pulling a TMF mass flow rate is usually around 0.047 SLPM. This is because fiber is made of pure silica and

has a softening temperature around 1700°C while the capillary is made of borosilicate which has a softening temperature around 800°C. If we use the mass flow rate of 0.047 SLPM with the borosilicate capillary, it just destroys it.

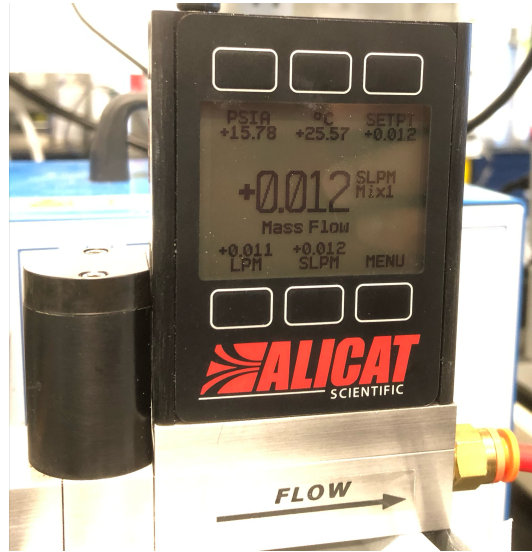


Figure 3.5: Hydrogen oxygen mass flow controller.

These parameters and the pulling recipe were determined experimentally by trial and error. The goal was to find parameters that will not melt the walls of the capillary but will only soften them the right amount so that they can be pulled. The parameters of the recipe were set to match the pulling to the softening of the walls so that they will maintain the pulling tension (figure 3.6) that will allow the material from the walls to draw outwards more so that the reduction of the internal diameter can be minimized and thinning of walls can be maximized.

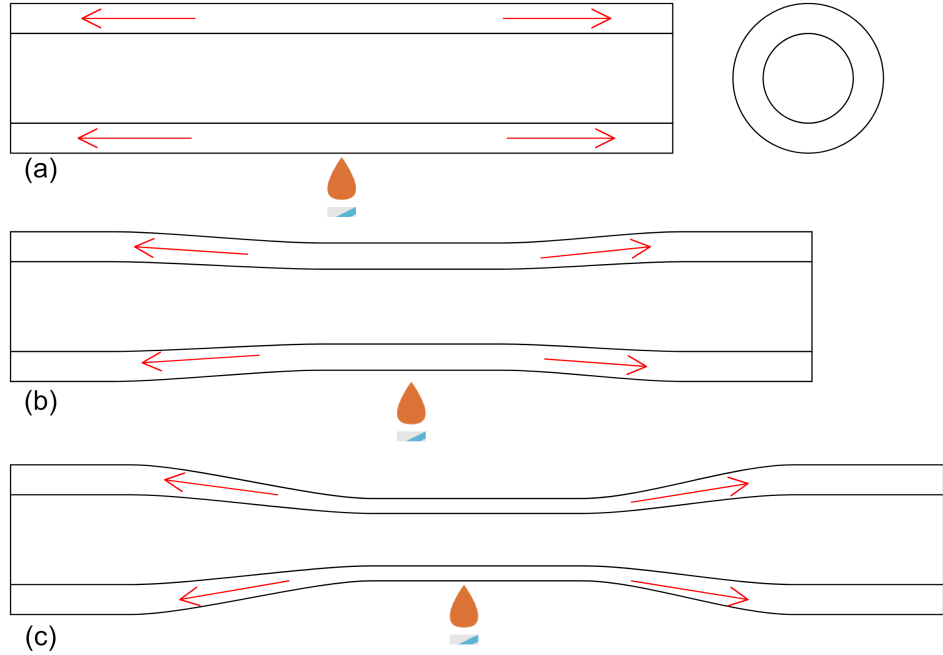


Figure 3.6: Pulling a Thin-walled hollow SNAP cavity from a off-the-shelf micro capillary. The capillary is pulled on a TMF setup over a hydrogen torch. Flame from the torch softens the capillary. As the capillary is pulled, the material from the walls draws outwards and wall thickness and capillary diameter is reduced. When the pulling stops, tension in capillary walls is released and nanoscale variations in the wall surface are formed.

Once the capillary was pulled, it was mounted (figure 3.7) on the light coupling and characterization setup and tested with and without water.

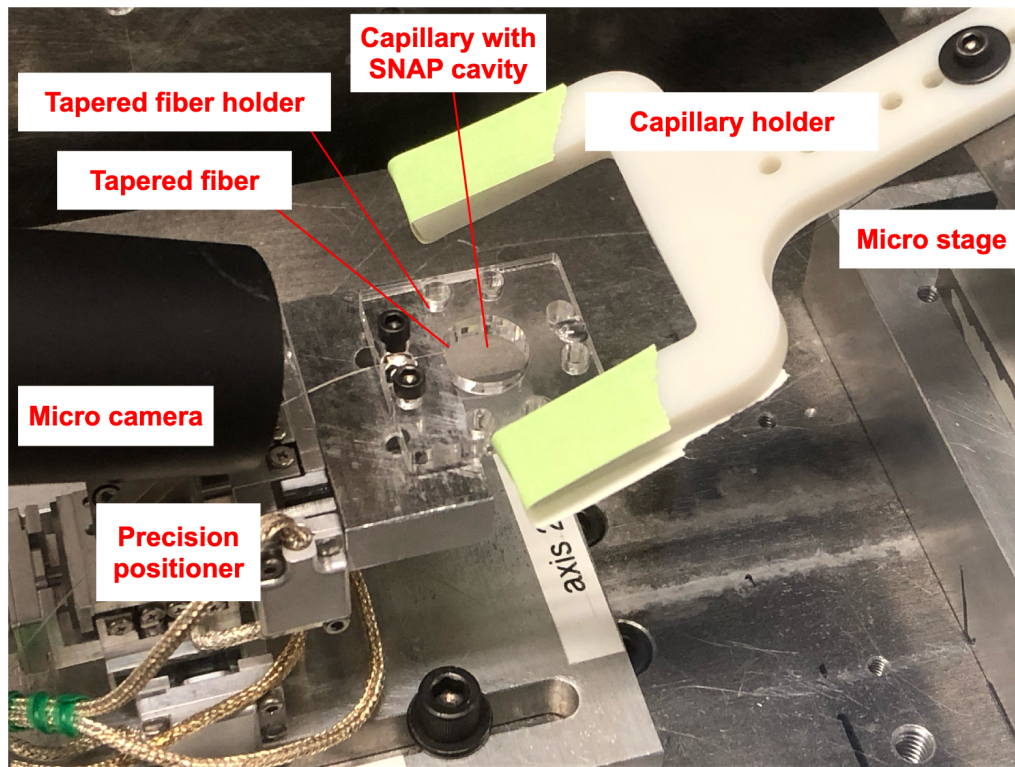


Figure 3.7: Light coupling and testing hollow SNAP cavity. Light was coupled using a TMF. To fill the capillary with the water a drop of water at room temperature was introduced at one end of the capillary and water was sucked in due to the capillary action.

We found out that when the wall of the capillary was reduced to just under 10 micrometers, the WGM resonance modes in the capillary walls could interact with water inside it (figure 3.10).

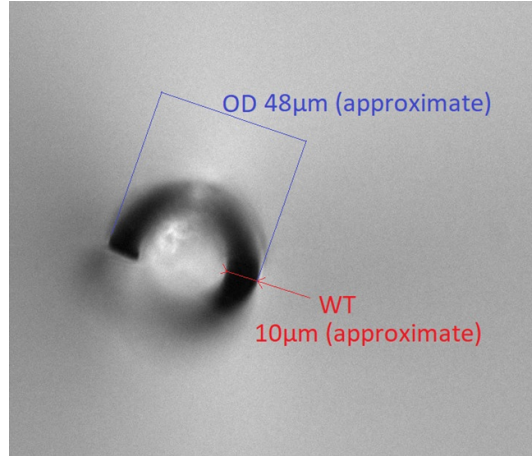


Figure 3.8: Pulled micro capillary with reduced diameter and reduced wall thickness. The outside diameter was reduced to approximately 48 micrometers, and the wall thickness was reduced to approximately 10 micrometers.

We started with an off-the-shelf borosilicate capillary with an outer diameter of 80 micrometers and wall thickness off 15 micrometers. We pulled the capillary for a length of six millimeters. In this process, the outside diameter was reduced to approximately 48 micrometers (figure 3.8) and the wall thickness was reduced to approximately 10 micrometers. We also found that the process of pulling the capillary also induced nanoscale variations in the surface of walls that can confine the light.

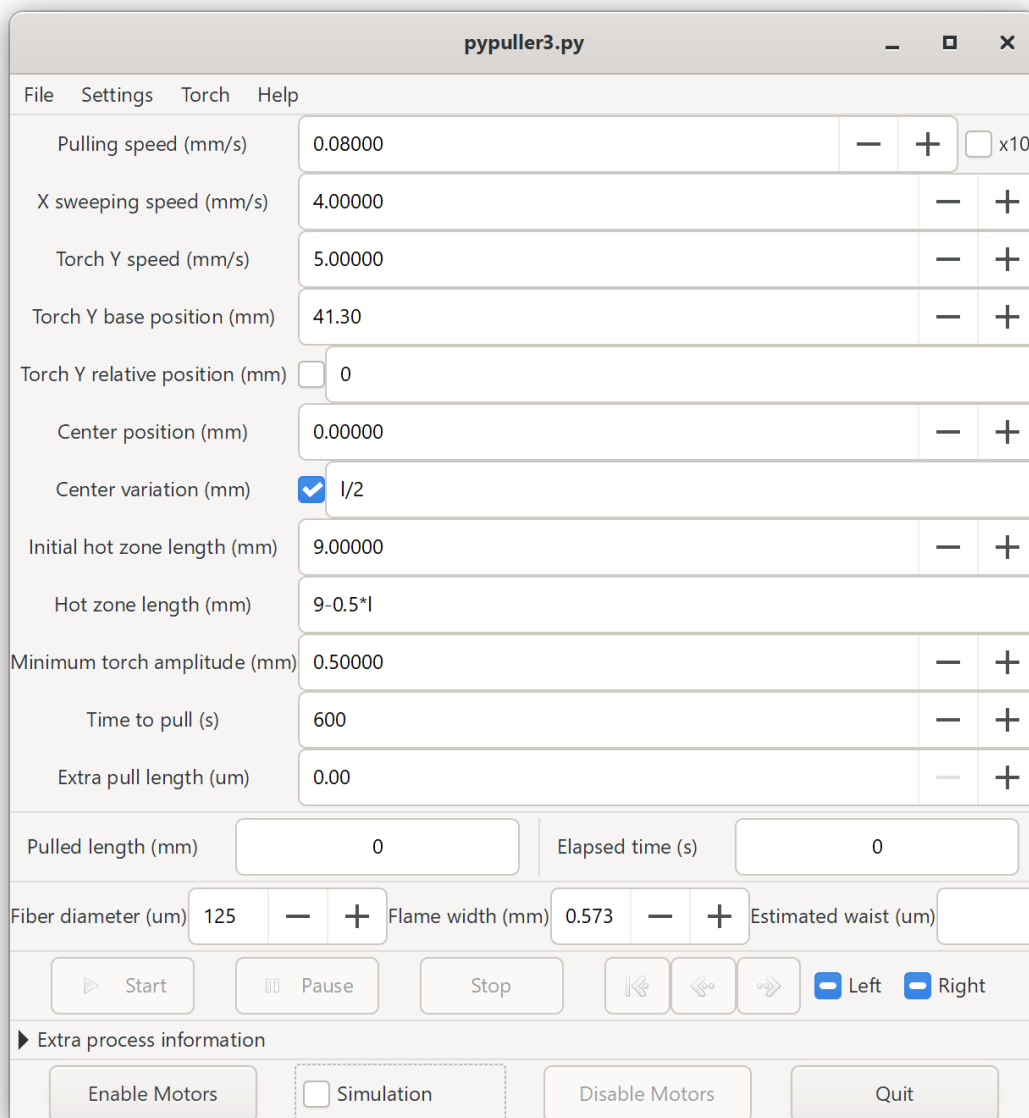


Figure 3.9: Tapered micro fiber pulling recipe.

For the reference figure 3.9 shows the recipe used to pull the TMF for these experiments. The mass flow used was 0.047 SLPM and the fiber was mounted 1.9 millimeters above the gauge 30 blunt needle.

3.4 Thin walled hollow WGM cavity as an water sensor

Figure 3.10 shows the final results of the experiment, and table 3.1 lists the parameters of modes 1, 2, and 3 before and after the capillary is filled with water. We first collected the transmission spectrum of the empty pulled capillary and then filled it with distilled water and collected the transmission spectrum again.

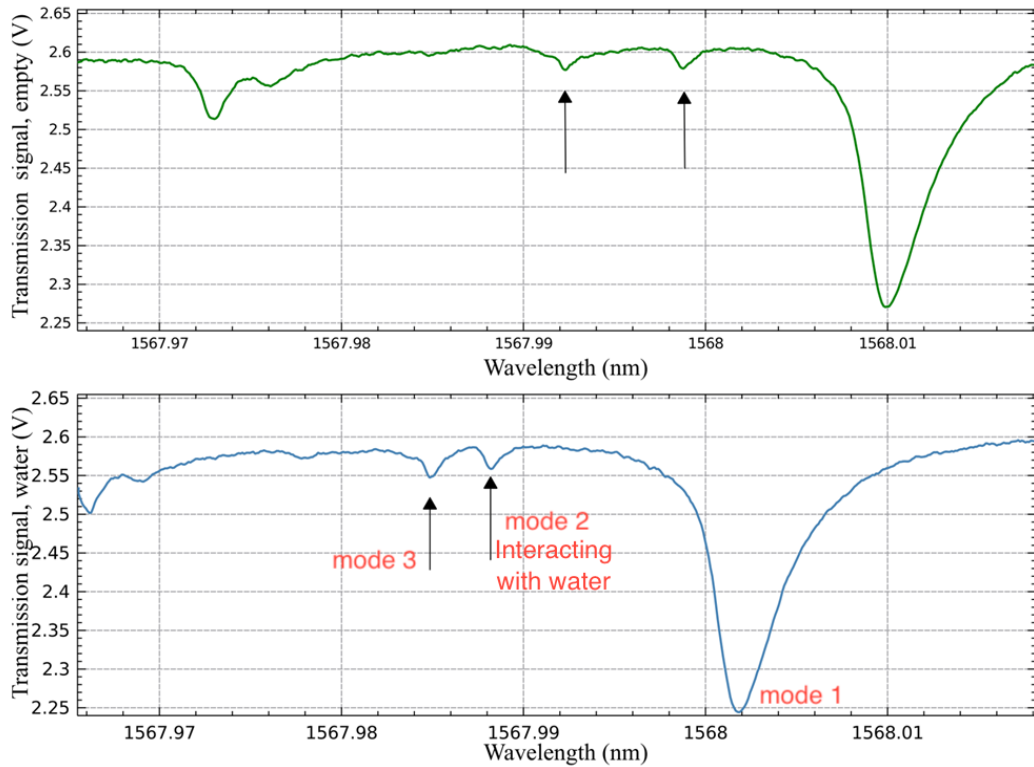


Figure 3.10: Resonance mode shift from water. Spectra of localized modes in a pulled capillary with and without water. Top panel: Spectrum of the empty capillary. Bottom panel: Spectrum after the capillary is filled with water. One of the arrows indicates the mode that is interacting with water.

	Mode	Center (nm)	Depth (V)	FWHM (nm)	Q	Shift (pm)	Q reduction
Air	1	1568.010525	0.12545800	0.003927210	0.3992683164×10^6		
	2	1567.998817	0.00820498	0.000422103	3.7147303312×10^6		
	3	1567.992390	0.00929153	0.001184670	1.3235689179×10^6		
Water	1	1568.002377	0.12866500	0.004294230	0.3651416848×10^6	-8.148	0.9
	2	1567.988292	0.01066350	0.000599625	2.6149481626×10^6	-10.525	0.7
	3	1567.984861	0.01348570	0.001927000	0.8136921956×10^6	-7.529	0.6

Table 3.1: The parameters of modes 1, 2, and 3 before and after the capillary is filled with water. Modes 1 and 3 have the blue shift of approximately 8 pm and 7.5 pm. Mode 2, that is interacting with water has a higher blue shift, approximately 10.5 pm. Q reduction is the Q reduction factor.

Water was kept in the lab at room temperature prior to the experiment so that both the water and the capillary were at the same room temperature so that the temperature does not affect the resonance modes. If colder or warmer water is filled into the capillary, the temperature change could also lead to a change in resonance mode. To fill the capillary with the water, a drop of water was introduced at one end of the capillary and water was sucked in due to the capillary action. Capillary was mounted horizontally so that there is no pressure gradient due to the gravity. There was no external pressure applied to the empty or the water filled capillary. Pressure inside and outside the capillary was in equilibrium at all the times.

The bottom panel of the figure 3.10 shows that when the capillary is filled with water, resonance modes shift to shorter wavelengths and become wider. There is a global blue shift of 7.5 pm to 8 pm except for the one mode that is interacting with water. The global blue shift of 7.5 pm to 8 pm could be related to calibration issues, but the mode that is interacting with water has a higher blue shift, approximately 10.5 pm.

This is due to the fact that air has a refractive index close to 1 and water is around 1.3. When the air inside the capillary is replaced by the water, the refractive index contrast between the cavity and the medium inside the cavity that this mode sees is reduced, leading to a reduction in the effective refractive index of the cavity for this mode. When the effective index is reduced, the optical path length is reduced and the resonance shifts to the shorter wavelength.

The resonance line width of this mode is also increased and Q-factor is reduced

because water is a strong absorber of infrared light; therefore it absorbs the energy from this mode, reduces its lifetime and leads to a wider resonance. The Q-factor of the mode is reduced approximately by 30%. This shows that at around ten micrometer cavity wall thicknesses, some resonance modes can extend beyond the internal surface of the hollow cavity and interact with the medium inside the cavity.

In conclusion, for this chapter, we have shown that we can make a thin-walled hollow SNAP cavity by using a hydrogen torch and a TMF pulling setup without using a carbon dioxide laser or HF etching. The SNAP cavity that we made can confine the light and the walls are thin enough that the electric field from resonance mode extends beyond the internal walls of the cavity and interacts with the medium (water) inside the cavity. This shows a proof of concept that thin-walled hollow SNAP cavities have potential to be used as an optical sensor.

Chapter 4

Transmission impulse response and light pulse dynamics of a WGM optical cavity

In the previous chapter, we discussed sensing with the capillary, and when looking at the resonance shift we were using the frequency domain. The frequency domain is not the only way we can measure properties of an optical cavity. Because the time domain is connected to the frequency domain, it is also possible to measure the properties of WGM cavities in the time domain [51]. Since we had access to an optical backscatter reflectometer (OBR), we decided to do some time domain measurements of a SNAP cavity to better understand its time response. In these experiments we have not done measurements for the sensing but in future, we can do measurements for the sensing as well.

In this chapter we present transmission impulse response and light pulse dynamics of a SNAP optical cavity measured by an OBR. OBR is used widely in the telecom industry for a variety of fiber-optic network and component test. OBR is used to detect faults in long underground or under sea optical cables. It sends a beam of light into the optical fiber and waits for the return of reflections. If there are any faults in the optical line, part of the beam will be reflected back to the OBR by the fault. It will use the time delay and the strength of the back reflected signal to determine the distance and type of fault.

For this experiment we used an optical circulator (Oplink, part number: MIOC15500031111) to route the light from OBR to a tapered microfiber (figure 4.1). The tapered microfiber was coupled to a SNAP cavity. The output of tapered

microfiber was connected back to the optical circulator. The purpose of an optical circulator is to route the light entering any port to the next port. This means that if light enters the port 1 it is routed to the port 2, light entering the port 2 is routed to the port 3, and so on. Since the OBR uses only one port to send optical signals and receive back reflections, we used an optical circulator to send output of TMF back to the port where OBR was connected.

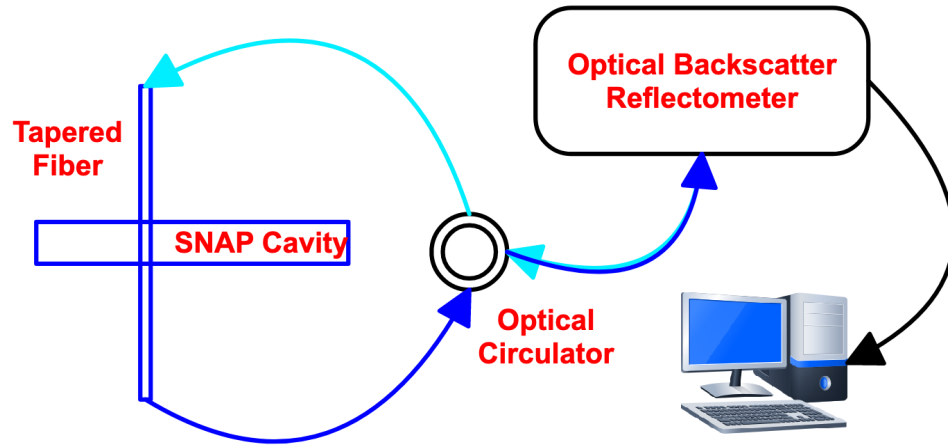


Figure 4.1: Impulse response and light pulse dynamics measurement setup.

The OBR that we used in this experiment was LUNA OBR 4600. Figure 4.2 shows the simplified diagram of the internal measurement method of a LUNA OBR[52]. Internally the OBR uses an interferometer, polarization controller, and a tunable laser. Light from the laser is split and sent to measurement arms of an interferometer and a polarization controller. Then a polarization beam splitter splits the light from the polarization controller evenly between two orthogonal polarization states. These polarization states are then interfered with the measurement field from the device or the fiber under test and are recorded at detectors labeled P and S. In essence, an OBR sends quasi continuous wave (CW) light at different wavelengths, and uses interference to find the complex amplitude of the reflected light. It then uses Fourier transform to convert this data to the time domain.

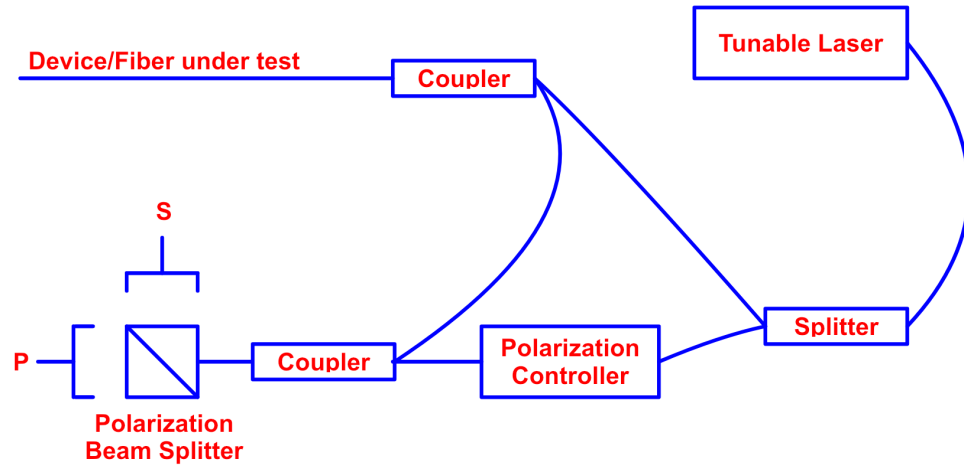


Figure 4.2: A simplified internal diagram of an optical backscatter reflectometry (OBR) measurement device.

The laser light that we used in our experiment was tuned over the range from 1525 nm to 1610 nm. The top panel of the figure 4.3 shows the transmission amplitude of the light sent out by the OBR that came back to the OBR. When we zoom on the peak, as shown in the bottom panel of the figure 4.3 we see the response of the cavity coupled to the tapered microfiber.

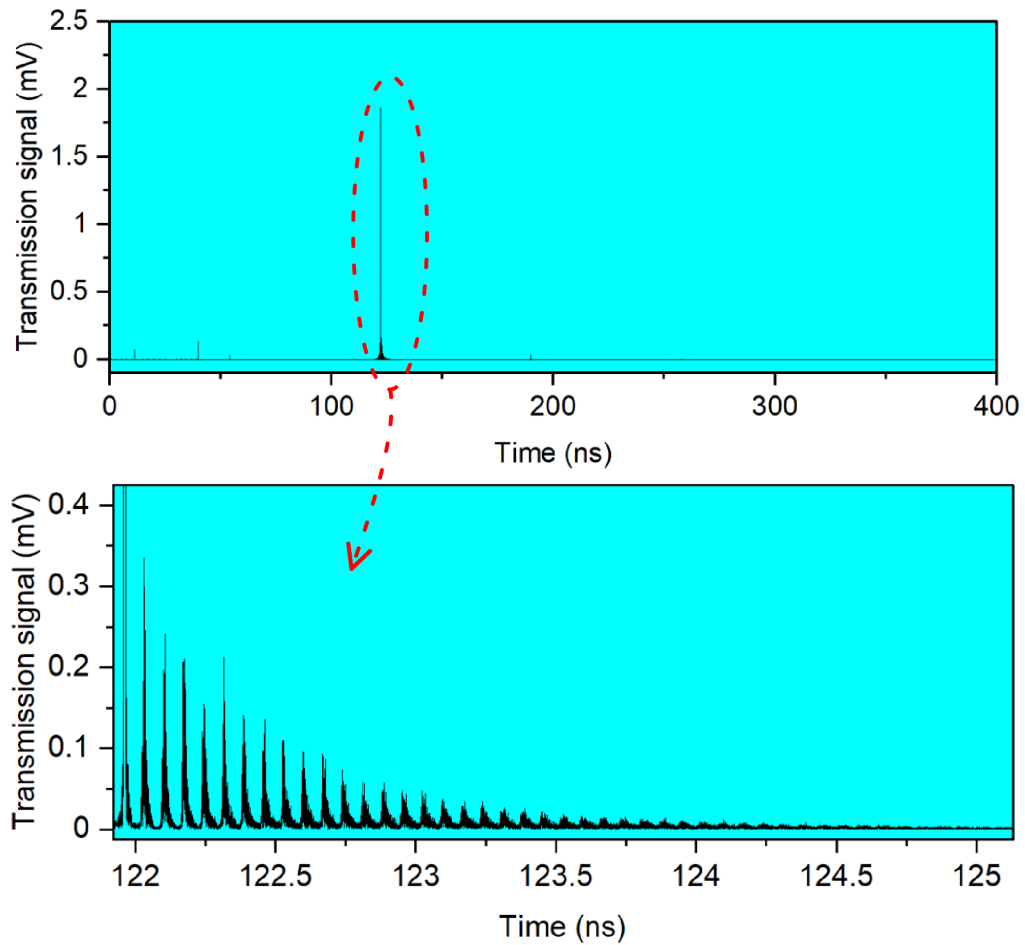


Figure 4.3: Transmission impulse response of a SNAP cavity. Top panel shows the transmission amplitude of the light sent out by the OBR that came back to the OBR. When we zoom on the peak as shown in the bottom panel, we see the response of the cavity coupled to the tapered microfiber.

Light is stored in the cavity and decays as it travels inside the cavity. The transmission trace shows that after every round trip, part of the light that is coupled into the cavity couples out of the cavity by coupling back to the tapered microfiber, this is why we see slowly decaying peaks in the transmission spectrum (figure 4.4). Peaks are spaced in time, and the time difference between peaks represents the round trip time of the light traveling inside the cavity. Data also shows the lifetime of the light in the SNAP cavity as the part of the light stored in the cavity is lost. After every round trip, the height of the peak is reduced. Part of the light is coupled back to tapered microfiber and part of it is lost to scattering and absorption by the cavity

medium.

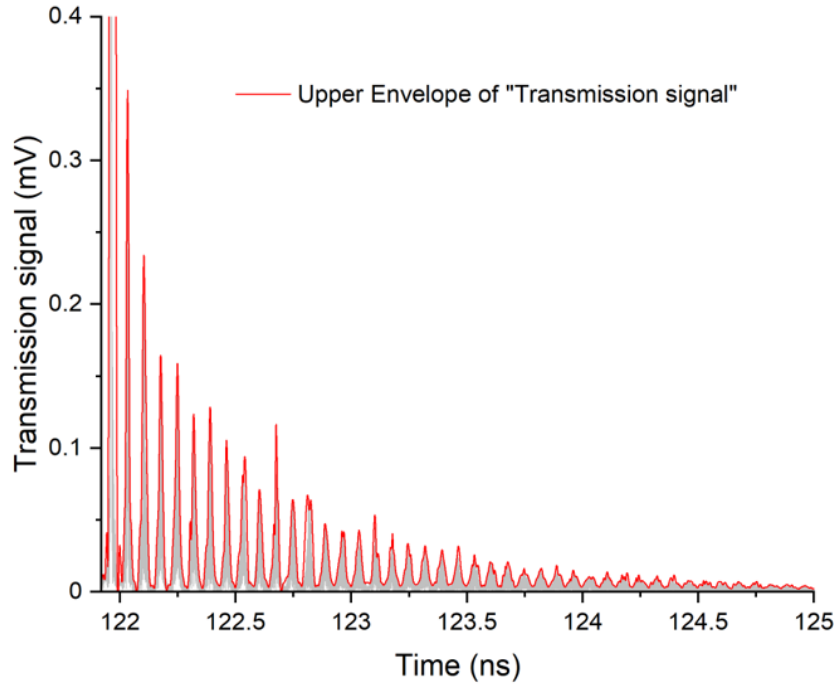


Figure 4.4: Transmission impulse response and light pulse dynamics measurement of a SNAP cavity. After every round trip, part of the light that is coupled into the cavity couples out of the cavity by coupling back to the tapered microfiber, this is why we see slowly decaying peaks in the transmission spectrum. Peaks are spaced in time, and the time difference between peaks represents the round trip time of the light traveling inside the cavity.

Next, as shown in figure 4.5, we coupled the tapered microfiber on the SNAP cavity at nine locations 0.2 mm apart and collected the data.

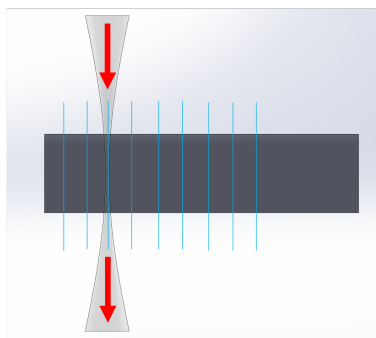


Figure 4.5: Collecting cavity response at nine locations 0.2 millimeters apart.

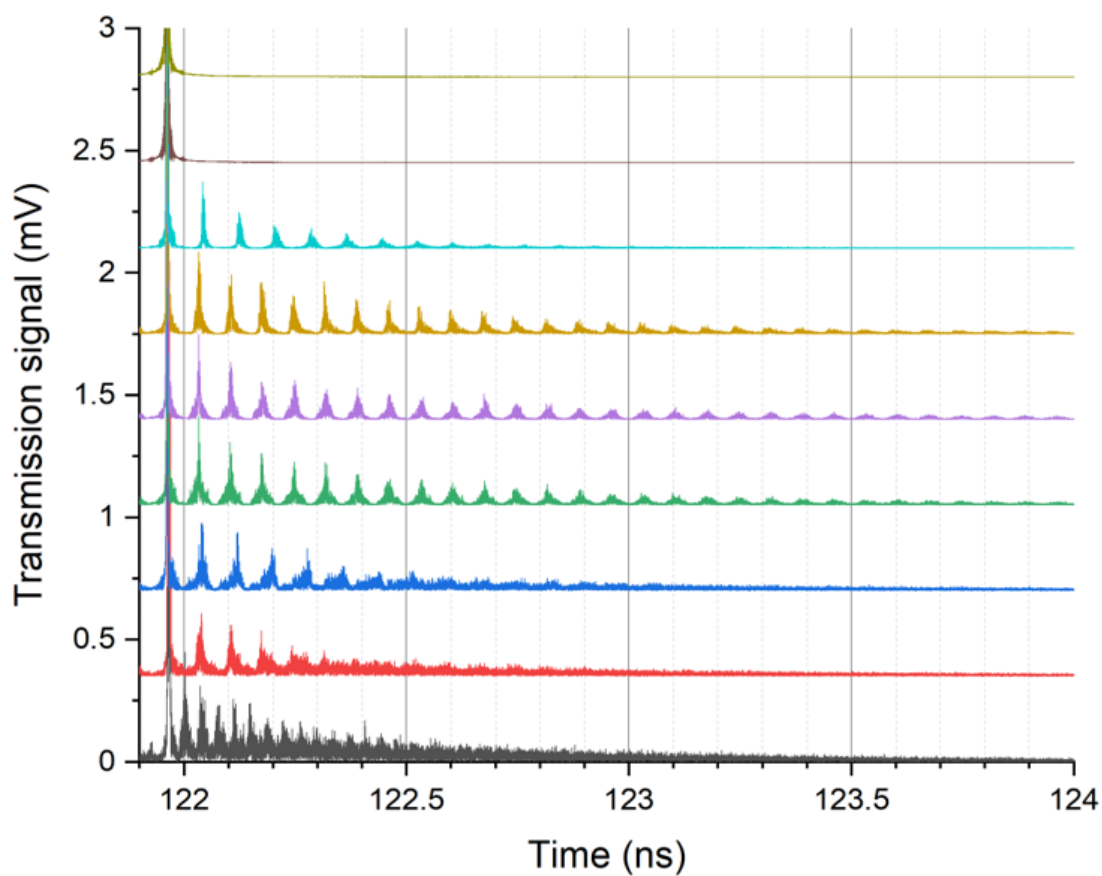


Figure 4.6: Transmission impulse response of a SNAP cavity at nine locations 0.2 mm apart. From bottom to top, transmission from location one at bottom and from nine at the top. At locations eight and nine (top two curves), the fiber does not have any cavity to confine the light; therefore there is no light coupled into these two locations.

Figure 4.6 shows the results of the measurements starting with the location one at bottom to the location nine at the top.

Data shows that at locations eight and nine (top two curves) the fiber does not have any cavity to confine the light, therefore there is no light coupled into these two locations. Light is coupled at another seven locations. For locations two to seven the measured round trip time of light from the data is approximately 70 ps to 80 ps, giving free spectral range from 12.5 GHz to 14.3 GHz. A round trip time of 70 ps to 80 ps also means that light (cavity refractive index 1.5) in a round trip traveled 1.4 cm to 1.6 cm on a helical path. Light coupled at location one (curve at bottom) has an approximate free spectral range of 28.6 GHz and round trip time of around 35 ps giving travel length per round trip around 0.7 cm. The cavity lifetime of light for all the locations is approximately 0.55 ns to 2 ns with the highest being at location five. This gives the Q-factor for the locations one to seven on the order of 10^5 .

In conclusion, for this chapter we have presented transmission impulse response and light pulse dynamics of a SNAP optical cavity. Data presented shows the lifetime of the light in the SNAP cavity as the light stored in cavity decays exponentially. The result of the measurement shows that after every round trip part of the light coupled into the SNAP cavity couples out of the cavity by coupling back to the tapered microfiber. Since the time domain is connected to the frequency domain, the time response measurements give us a way to determine the same quantities as spectral measurements, and could be useful for sensing.

Chapter 5

Conclusion

In conclusion, in this thesis we discussed the theory and the applications of WGM cavities. We have shown that we can make a thin-walled hollow SNAP cavity by using a hydrogen torch and a TMF pulling setup without using a carbon dioxide laser or HF etching. The SNAP cavity that we made can confine the light and the walls are thin enough that the electric field from resonance mode extends beyond the internal walls of the cavity and interacts with the medium (water) inside the cavity. When resonance mode interact with water, it becomes wider and shifts to the shorter wavelength. It shows a proof of concept that thin-walled hollow SNAP cavities have potential to be used as an optical sensor.

We also present transmission impulse response and light pulse dynamics of a SNAP optical cavity. Data presented shows the lifetime of the light in the SNAP cavity as the light stored in cavity decays exponentially. The result of the measurement shows that after every round trip part of the light coupled into the SNAP cavity couples out of the cavity by coupling back to the tapered microfiber.

For future work, we can further optimize capillary pulling recipes so that walls can be thin down to five micrometers or less so that more resonance modes will extend inside and interact with the medium inside the capillary. We can also work on functionalizing the internal surface so that a specific bio agent will bind to it and cavity can be used as an optical sensor for this agent. Another potential project would be to use the capillary to detect the change in concentration of gas inside the capillary. This would use the mode broadening mechanism. We expect the modes that coincide with absorption lines of gas will become broader when the gas concentration is increased. Furthermore we can also work on sensing using the time domain. The time response data that we collected with the OBR is very rich, and we are going to analyze it in more detail.

References

- [1] P. Bianucci, [Sensors](#) **16**, 1841 (2016).
- [2] A. Matsko and V. Ilchenko, [IEEE Journal of Selected Topics in Quantum Electronics](#) **12**, 3 (2006).
- [3] V. Ilchenko and A. Matsko, [IEEE Journal of Selected Topics in Quantum Electronics](#) **12**, 15 (2006).
- [4] M. Sumetsky, [Progress in Quantum Electronics](#) **64**, 1 (2019).
- [5] Toropov N, Cabello G, Serrano Mp, Gutha Rr, Rafti M, and Vollmer F, [Light, Science & Applications](#) **10**, 42 (2021).
- [6] L. Chang, M. de Goede, M. Dijkstra, C. I. van Emmerik, and S. M. García-Blanco, [Optics Express](#) **29**, 1371 (2021).
- [7] D. V. Strekalov, C. Marquardt, A. B. Matsko, H. G. L. Schwefel, and G. Leuchs, [Journal of Optics](#) **18**, 123002 (2016).
- [8] Q. Yu, Z. Zhang, and X. Shu, [Optics Letters](#) **46**, 1005 (2021).
- [9] M. Sumetsky, M. Sumetsky, S. Zaki, and S. Zaki, [Optics Letters](#) **46**, 3227 (2021).
- [10] M. Sumetsky, [Optics Letters](#) **46**, 4144 (2021).
- [11] G. Gardosi, B. J. Mangan, G. S. Puc, and M. Sumetsky, [ACS Photonics](#) **8**, 436 (2021).
- [12] Q. Yu, Q. Yu, S. Zaki, Y. Yang, N. Toropov, X. Shu, and M. Sumetsky, [Optics Letters](#) **44**, 5606 (2019).
- [13] K. V. Tokmakov and M. Sumetsky, in [2019 Conference on Lasers and Electro-Optics Europe European Quantum Electronics Conference \(CLEO/Europe-EQEC\)](#) (June 2019), pp. 1–1.
- [14] D. Bochek, N. Toropov, I. Vatnik, D. Churkin, and M. Sumetsky, [Optics Letters](#) **44**, 3218 (2019).

- [15] V. S. Ilchenko, A. A. Savchenkov, A. B. Matsko, and L. Maleki, *JOSA A* **20**, 157 (2003).
- [16] J. B. Khurgin, *Advances in Optics and Photonics* **2**, 287 (2010).
- [17] M. Sumetsky, *Optics Letters* **39**, 1913 (2014).
- [18] M. Sumetsky, *Physical Review Letters* **111**, 163901 (2013).
- [19] M. Sumetsky, *Scientific Reports* **5**, 18569 (2015).
- [20] V. Dvoyrin and M. Sumetsky, *Optics Letters* **41**, 5547 (2016).
- [21] L. Rayleigh, *The London, Edinburgh, and Dublin Philosophical Magazine and Journal of Science* **20**, 1001 (1910).
- [22] Femtoquake, *Picture of St Paul's whispering gallery taken on Oct. 31, 2012 during a private visit. CC BY-SA 3.0*, Oct. 31, 2011.
- [23] Author Unknown (public domain), *John William Strutt, 3rd Baron of Rayleigh, British physicist*. 1921.
- [24] R. D. Richtmyer, *Journal of Applied Physics* **10**, 391 (1939).
- [25] Jia-ming Liu, *Photonic Devices* (Cambridge University Press, Cambridge, 2005).
- [26] W. Bogaerts, P. De Heyn, T. Van Vaerenbergh, K. De Vos, S. Kumar Selvaraja, T. Claes, P. Dumon, P. Bienstman, D. Van Thourhout, and R. Baets, *Laser & Photonics Reviews* **6**, 47 (2012).
- [27] M. Sumetsky and J. M. Fini, *Optics Express* **19**, 26470 (2011).
- [28] A. A. Savchenkov, A. B. Matsko, V. S. Ilchenko, and L. Maleki, *Optics Express* **15**, 6768 (2007).
- [29] J. C. Knight, G. Cheung, F. Jacques, and T. A. Birks, *Optics Letters* **22**, 1129 (1997).
- [30] D. R. Rowland and J. D. Love, *IEE Proceedings J (Optoelectronics)* **140**, 177 (1993).
- [31] T. Birks and Y. Li, *Journal of Lightwave Technology* **10**, 432 (1992).
- [32] M. Sumetsky, *Nanophotonics* **2**, 393 (2013).
- [33] T. Hamidfar, "Fabrication and characterization of surface nanoscale axial photonics microresonators", MA thesis (Concordia University, Apr. 15, 2015), 123 pp.

- [34] F. Vollmer, S. Arnold, and D. Keng, [Proceedings of the National Academy of Sciences of the United States of America](#) **105**, 20701 (2009).
- [35] V. R. Dantham, S. Holler, C. Barbre, D. Keng, V. Kolchenko, and S. Arnold, [Nano Letters](#) **13**, 3347 (2013).
- [36] F. Vollmer, D. Braun, A. Libchaber, M. Khoshsima, I. Teraoka, and S. Arnold, [Applied Physics Letters](#) **80**, 4057 (2002).
- [37] M. R. Foreman, J. D. Swaim, and F. Vollmer, [Advances in Optics and Photonics](#) **7**, 168 (2015).
- [38] C. Z. Tan and J. Arndt, [Journal of Physics and Chemistry of Solids](#) **61**, 1315 (2000).
- [39] L. Shao, X.-F. Jiang, X.-C. Yu, B.-B. Li, W. R. Clements, F. Vollmer, W. Wang, Y.-F. Xiao, and Q. Gong, [Advanced Materials](#) **25**, 5616 (2013).
- [40] Y. Hu, L. Shao, S. Arnold, Y.-C. Liu, C.-Y. Ma, and Y.-F. Xiao, [Physical Review A](#) **90**, 043847 (2014).
- [41] B.-Q. Shen, X.-C. Yu, Y. Zhi, L. Wang, D. Kim, Q. Gong, and Y.-F. Xiao, [Physical Review Applied](#) **5**, 024011 (2016).
- [42] A. M. Armani and K. J. Vahala, [Optics Letters](#) **31**, 1896 (2006).
- [43] J. Zhu, S. K. Ozdemir, Y.-F. Xiao, L. Li, L. He, D.-R. Chen, and L. Yang, [Nature Photonics](#) **4**, 46 (2010).
- [44] L. He, S. K. Özdemir, Y.-F. Xiao, and L. Yang, [IEEE Journal of Quantum Electronics](#) **46**, 1626 (2010).
- [45] L. He, Ş. K. Özdemir, J. Zhu, F. Monifi, H. Yilmaz, and L. Yang, [New Journal of Physics](#) **15**, 073030 (2013).
- [46] D. S. Weiss, V. Sandoghdar, J. Hare, V. Lefèvre-Seguin, J.-M. Raimond, and S. Haroche, [Optics Letters](#) **20**, 1835 (1995).
- [47] X. Yi, Y.-F. Xiao, Y. Feng, D.-Y. Qiu, J.-Y. Fan, Y. Li, and Q. Gong, [Journal of Applied Physics](#) **111**, 114702 (2012).
- [48] Y. Louyer, D. Meschede, and A. Rauschenbeutel, [Physical Review A](#) **72**, 031801 (2005).
- [49] I. M. White, H. Oveys, and X. Fan, [Optics Letters](#) **31**, 1319 (2006).
- [50] H. Ghali, “Optical Microcavities for Real-Time Detection of Bacteria”, PhD thesis (Université de Montréal, June 2016).

- [51] H. Bergeron, J.-R. Carrier, V. Michaud-Belleau, J. Roy, J. Genest, and C. N. Allen, [Physical Review A](#) **87**, 063835 (2013).
- [52] Lune Inc, *Optical Backscatter Reflectometry (OBR) Overview and Applications*.